Molecular Therapy
Oncolytics
Original Article

Adenoviral delivery of an immunomodulatory protein to the tumor microenvironment controls tumor growth

Patrick O'Connell,[1] Maja K. Blake,[1] Yuliya Pepelyayeva,[1] Sean Hyslop,[1] Sarah Godbehere,[1] Ariana M. Angarita,[1] Cristiane Pereira-Hicks,[1] Andrea Amalfitano,[1,2] and Yasser A. Aldhamen[1]

[1]Department of Microbiology and Molecular Genetics, College of Osteopathic Medicine, Michigan State University, 567 Wilson Road, 4194 Biomedical and Physical Sciences Building, East Lansing, MI 48824, USA; [2]Department of Pediatrics, College of Osteopathic Medicine, Michigan State University, East Lansing, MI 48824, USA

Targeted modulation of the immune system against tumors can achieve responses in otherwise refractory cancers, which has spurred efforts aimed at optimizing such strategies. To this end, we have previously investigated cancer immunotherapy approaches using recombinant adenovirus vectors, as well as via modulation of the self-ligand receptor SLAMF7. Here, we present a gene transfer-based immunotherapy approach using targeted expression of a SLAMF7-Fc fusion construct directly into tumors at high concentrations via a recombinant adenoviral vector (Ad-SF7-Fc). Using multiple murine cancer models, we show that Ad-SF7-Fc can induce tumor control via augmentation of innate immunity; specifically, induction of type I interferons and activation of dendritic cells (DCs) and macrophages. Analogously, we find that modulating SLAMF7 signaling via an adenoviral vector expressing its intracellular adaptor, EAT-2, is also capable of inducing tumor control. Finally, we employ a novel *in vivo* prediction approach and dataset integration with machine learning to dissect how Ad-SF7-Fc modulates cell-type-specific responses in the tumor microenvironment to achieve tumor control. Thus, our novel combinatorial cancer immunotherapy highlights the benefit of multimodal immune modulation and lays a framework for combination with complementary approaches capable of inducing adaptive immune responses.

INTRODUCTION

Cancer immunotherapy has revolutionized the way we think about cancer from both treatment and research perspectives.[1] Currently, the most clinically successful approaches to antagonize the immune system against tumors rely on the use of monoclonal antibodies which, for the most part, modulate T cell responses.[2] While highly efficacious in subsets of patients with certain cancers,[1,2] these antibodies still suffer a number of limitations, not limited to: their non-selective targeting of immune cells systemically, induction of autoimmunity,[3] development of resistance,[4] high production cost, and exaggerated adverse effects when used in combination.[5] As an alternative approach to induce anti-cancer immune responses, recombinant viral vectors have been investigated, including a number of studies and clinical trials using human recombinant adenovirus vectors.[6,7] These viral approaches function via multiple mechanisms including direct cytolysis of tumor cells and augmentation of anti-tumor immune responses,[7] but have fallen short of the impressive responses produced by monoclonal antibodies.[1,2] Combining antibody-based and viral-based approaches has the potential to address a number of the issues faced by these individual therapies.

The signaling lymphocytic activation molecule family member 7 (SLAMF7) (CRACC, CD319, CS-1) is a self-ligand receptor, restricted to hematopoietic cells and expressed at varying frequencies on different immune cell subsets.[8–10] SLAMF7 is capable of mediating both activating and inhibitory signals in immune cells; a distinction largely dependent on the presence of its adaptor protein, Ewing's sarcoma-associated transcript 2 (EAT-2).[11] When SLAMF7 is activated in the presence of EAT-2, EAT-2 binds to SLAMF7's phosphorylated intracellular immunoreceptor tyrosine-based switch motif (ITSM) and mediates immune cell activation, while in the absence of EAT-2, various inhibitory SH2 domain-containing phosphatases are recruited to SLAMF7's ITSM.[11,12] We recently demonstrated that SLAMF7 activation in type I interferon stimulated monocytes, which lack EAT-2, results in inhibition of pro-inflammatory chemokine responses.[8] We also found that SLAMF7 signaling on $CD8^+$ T cells reprograms them toward an exhausted phenotype, a finding of particular relevance to cancer immunotherapy.[10] A number of studies have also described various roles for SLAMF7 on natural killer (NK) cell and dendritic cell (DC) activation/function[11–13] that, considering how important functions of these two cell types are to tumor control, suggest therapeutically targeting SLAMF7 could affect anti-tumor immune responses.

Received 22 September 2021; accepted 4 December 2021;
https://doi.org/10.1016/j.omto.2021.12.004.

Correspondence: Yasser Ali Aldhamen, PhD, Michigan State University, 567 Wilson Road, 4194 Biomedical and Physical Sciences Building, East Lansing, MI 48824, USA
E-mail: aldhamen@msu.edu

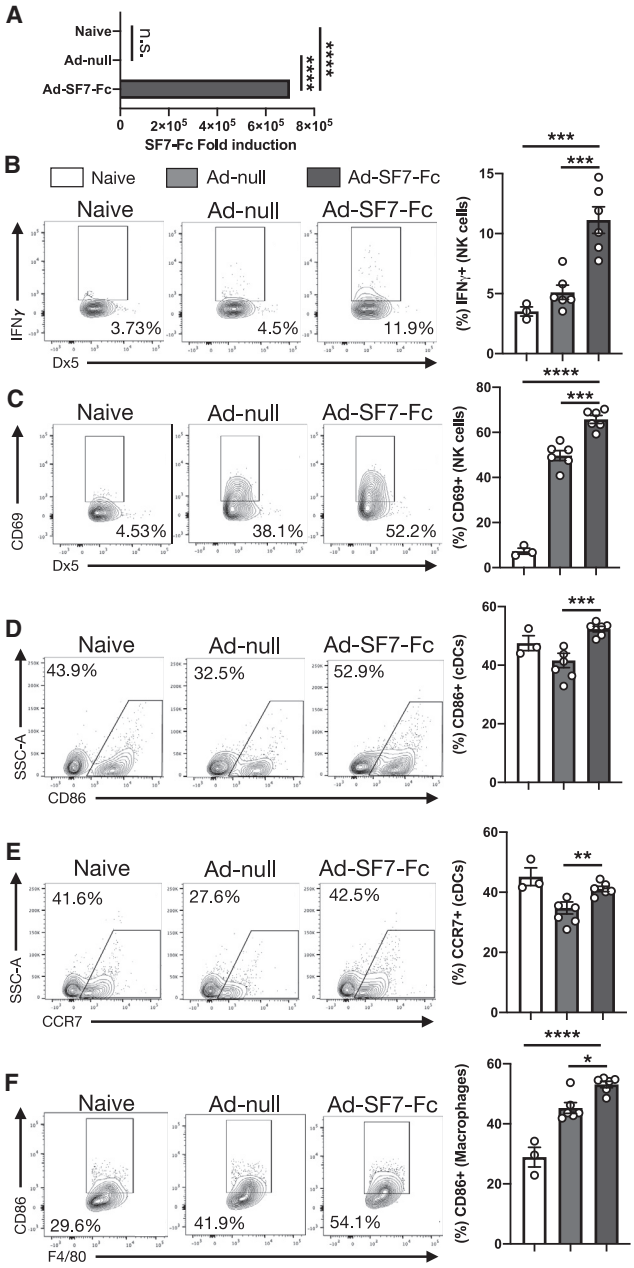

Figure 1. Ad-SF7-Fc expresses SF7-Fc and activates NK cells and DCs

(A) HEK-293-C7 cells (n = 3) were control treated with PBS (naive) or infected at an MOI of 1 × 10^3 with Ad-null or Ad-SF7-Fc overnight and *SLAMF7* gene expression was assessed. BALB/c mice were injected I.V. with 1 × 10^{10} v.p. of Ad-null (n = 6), Ad-SF7-Fc (n = 6), or not injected (naive, n = 3), spleens were harvested 10 h later and immune cell phenotype was analyzed by flow cytometry. (B) IFNγ production by NK cells. (C) CD69 expression on NK cells. (D) CD86 expression on cDC cells. (E) CCR7 expression on cDC cells. (F) CD86 expression on macrophages. All data presented as mean ± standard error of the mean and representative of a single experiment. Groups compared with one-way ANOVA with Tukey's multiple comparison test. *p < 0.05; **p < 0.01; ***p < 0.001; ****p < 0.0001; n.s. = not significant.

Extending these findings, we recently demonstrated that targeting SLAMF7 using a SLAMF7-Fc (CRACC-Fc, SF7-Fc) fusion protein enhanced natural killer cell (NK) cell and DC activation.[14] Therefore, we hypothesized that a recombinant adenovirus vector-expressing SLAMF7-Fc (Ad-SF7-Fc) may augment anti-tumor responses via localized immune activation from both the adenovirus vector and SLAMF7-Fc, while delivering high levels of SLAMF7-Fc to the tumor microenvironment (TME) in a targeted, cost-effective manner. Through testing Ad-SF7-Fc across multiple murine cancer models, we found this integrated immunotherapy capable of augmenting innate immune responses and concordantly controlling tumor growth. Novel *in vivo* prediction approaches confirm Ad-SF7-Fc can enhance pro-inflammatory DC responses and suggest that SLAMF7 activation on plasmacytoid DCs (pDCs) may be particularly efficacious in inducing anti-tumor immunity. Finally, we use a machine learning-based approach to identify the factors critical to tumor control by Ad-SF7-Fc.

RESULTS

Ad-SF7-Fc induces high expression of SF7-Fc and activates the innate immune system

While we found that our SF7-Fc fusion protein was able to modulate SLAMF7 signaling and induce innate immune activation,[14] the production of large amounts of recombinant proteins like SF7-Fc is expensive and delivery to specific locations challenging.[15,16] To address this, we constructed a recombinant, replication deficient adenovirus vector capable of expressing SF7-Fc (Ad-SF7-Fc). We first confirmed the ability of Ad-SF7-Fc to express SF7-Fc by infecting HEK293 cells (Figure 1A).

Previously, we found co-administration of SF7-Fc fusion protein and Ad-null increased IFNγ production by NK cells.[14] Here, we found that treatment with Ad-SF7-Fc increased IFNγ production and CD69 expression on NK cells compared with the Ad-null control (Figures 1B and 1C). Since we also found that SF7-Fc was capable of activating DCs,[14] we further investigated DC responses after treatment with Ad-SF7-Fc. We observed increased DC maturation as evidenced by increased CD86 (Figure 1D) and CCR7 (Figure 1E) expression on DCs, along with increased CD86 expression on macrophages (Figure 1F). Additionally, Ad-SF7-Fc was able to augment immune cell activation on B cells, $CD8^+$ T cells, and $CD4^+$ T cells (Figures S1A–S1C).

Ad-SF7-Fc augments cytokine and type I interferon responses

To investigate the impact of Ad-SF7-Fc on cytokine responses, we evaluated splenic gene expression in mice 6 h after vector injection. We found up-regulation of *Il12*, *Csf2* (GM-CSF), and *Il6* (Figure 2A). Interestingly, Ad-SF7-Fc decreased expression of *CXCL10* (IP-10) compared with Ad-null (Figure 2A), suggesting SF7-Fc may be activating SLAMF7 on monocytes; a result consistent with our previous work.[8] Since NK cell activation is mediated by type I interferons and we previously found that SLAMF7 is both an IFN responsive gene and modulator of specific IFN responses, we investigated if Ad-SF7-Fc could augment type I IFN responses. In comparison

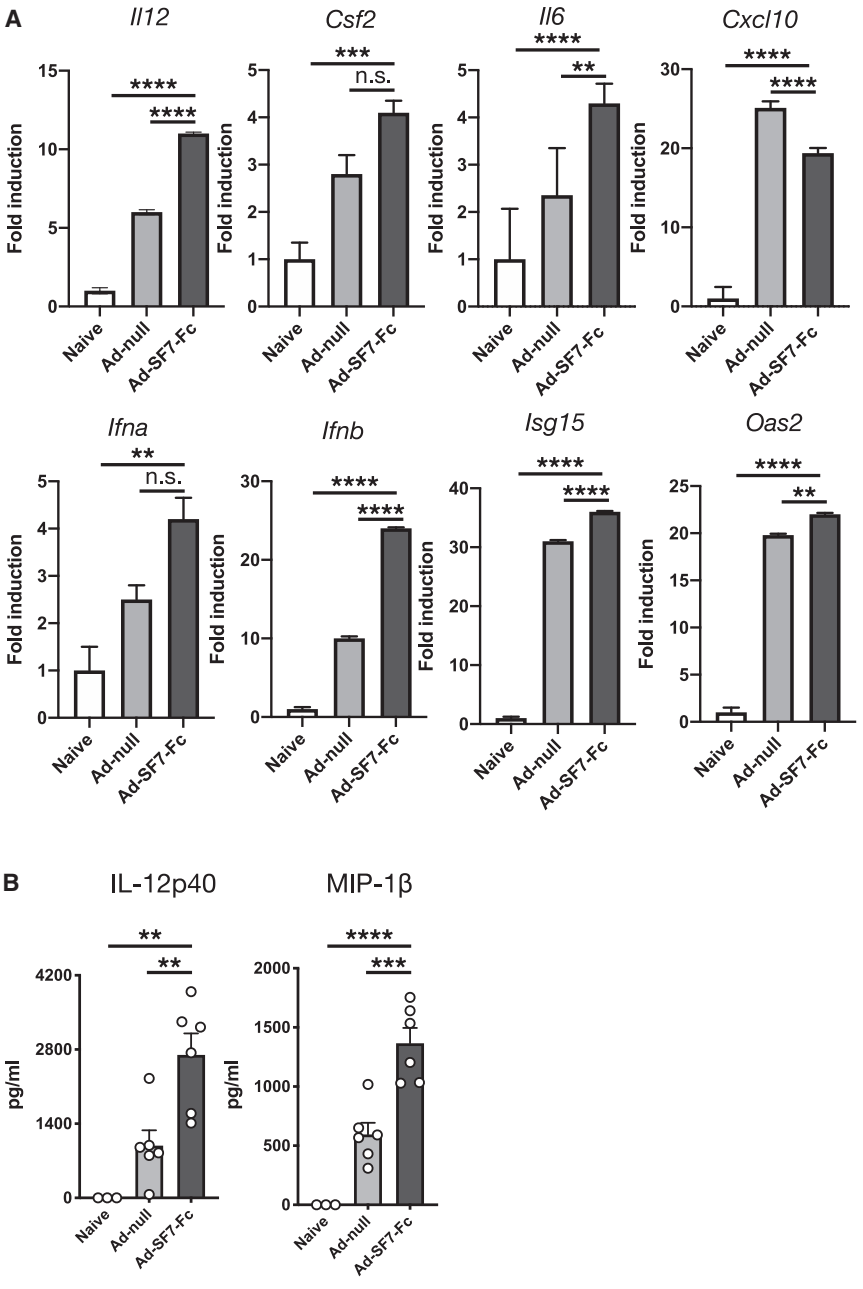

Figure 2. Ad-SF7-Fc induces a proinflammatory cytokine and IFN response

(A) BALB/c mice were injected I.V. with 1×10^{10} v.p. of Ad-null, Ad-SF7-Fc, or not injected (naive) and 6 h later spleens were collected for RNA analysis. (B) Plasma levels of IL-12(p40) and MIP-1β were compared across treatment groups. All data presented as mean ± standard error of the mean and representative of a single experiment. Groups compared with one-way ANOVA with Tukey's multiple comparison test. **p < 0.01; ***p < 0.001; ****p < 0.0001; n.s. = not significant.

with Ad-null-treated mice, we detected increased expression of *Ifna*, *Ifnb*, *Isg15*, and *Oas2* in Ad-SF7-Fc-treated mice (Figure 2A). Furthermore, we detected increased IL-12(p40) and MIP-1β (CCL4) proteins in the plasma of Ad-SF7-Fc-treated mice compared with Ad-null-treated controls (Figure 2B).

Ad-SF7-Fc controls CT26 tumor growth in the absence of humoral immune responses

To examine whether Ad-SF7-Fc induces anti-tumor responses *in vivo* we used the CT26 mouse model. We first confirmed successful expression of SF7-Fc in CT26 cells *in vitro* (Figures 3A and S3A) and *in vivo* (Figure 3B). Then, we treated established CT26 tumors intra-tumorally (I.T.) with Ad-null, Ad-SF7-Fc, or untreated (naive). We found significantly increased survival in Ad-SF7-Fc treated mice (Figure 3C) and decreased tumor volume in Ad-SF7-Fc treated as compared with Ad-null treated tumors (Figure 3D).

To determine whether the tumor control we observed was due to an increased adaptive immune response, we investigated if an abscopal effect[17] was present in our CT26 model. To explore whether Ad-SF7-Fc could induce an abscopal effect we implanted two CT26 tumors in the hind flanks of mice and treated one side twice with Ad-null or Ad-SF7-Fc (Figures 3D and 3E). We not only found superior tumor control in tumors directly injected with Ad-SF7-Fc (Figure 3D), but also noted that the contralateral tumors in mice receiving Ad-SF7-Fc had superior tumor control compared with mice receiving Ad-null (Figure 3E). This indicates that an abscopal effect is present in mice treated with Ad-SF7-Fc. These data also suggest that the modulation of SLAMF7 functions by Ad-SF7-Fc induces a memory immune response against CT26 tumors. We also assessed tumor antigen-specific B cell memory responses to determine if the adaptive response was humoral in nature. Mice were co-vaccinated with various adenovirus vectors and CT26 tumor lysate. We found Ad-SF7-Fc/CT26 lysate co-vaccinated mice produced only slightly higher levels of CT26-specific antibodies compared with Ad-null/CT26 lysate (Figure S3B). To measure the functionality of these antibodies, we performed antibody-dependent cellular cytotoxicity (ADCC) assays using plasma from the vaccinated mice, carboxyfluorescein succinimidyl ester (CFSE)-labeled CT26 cells, and either total splenocytes (Figure 3F) or isolated NK cells (Figure 3G). We found no significant difference between cultures using

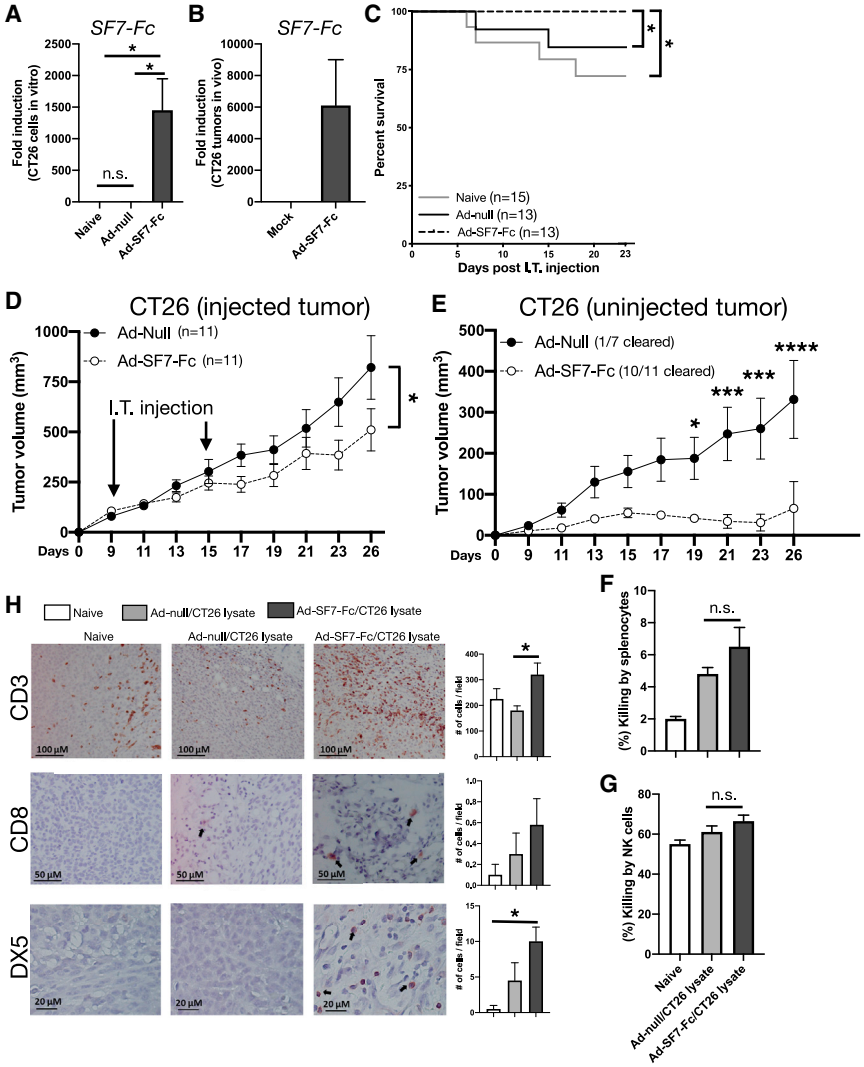

Figure 3. Control of CT26 tumor growth by Ad-SF7-Fc in the absence of an increased humoral immune response

(A) CT26 cells were untreated (naive) (n = 3) or infected at an MOI of $1x10^3$ with Ad-null (n = 3) or Ad-SF7-Fc (n = 3) virus overnight. mRNA was isolated from cells and *SLAMF7* expression was assessed. (B) BALB/c mice were injected S.Q. in the flank with 1.5×10^5 CT26 cells and 14 days later mice were injected I.T. with 1×10^{10} v.p. of Ad-SF7-Fc (n = 2) or not injected (naive) (n = 2). Tumors were harvested 14 h later and *SLAMF7* gene expression was assessed. BALB/c mice were injected S.Q. with $1.5x10^5$ CT26 cells and eight days later mice were split into three groups: Ad-null (n = 13), Ad-SF7-Fc (n = 13), and not injected (naive, n = 15). All viruses were injected I.T. (C) Kaplan-Meier survival curve of virus treated CT26 tumor-bearing mice. Tumors were injected once. (D) Tumor volumes in a second cohort of CT26 tumor-bearing mice. Mice were inoculated on both hind flanks with CT26 cells and one tumor was injected I.T. with virus on days 9 and 15. (E) Tumor volumes of the uninjected tumor from (D). Splenocytes (F) or NK cells (G) from naive mice were incubated with CFSE labeled CT26 cells and cultured in presence of plasma from Ad-null/CT26 lysate vaccinated, Ad-SF7-Fc/CT26 lysate vaccinated, or non-vaccinated mice. CT26 viability was assessed by flow cytometry to determine percent killing. (H) CT26 tumors were harvested from mice used in (F and G) and IHC was performed for CD3, CD8, and DX5. Data from (A, B, and F–H) presented as mean ± standard error of the mean and representative of a single experiment. Data in (C–E) representative of two independent experiments showing similar results. Groups in (A, F, G, and H) were compared with one-way ANOVA with Tukey's multiple comparison test. The log rank test used to compare groups in (C). A two-way ANOVA with Sidak's post-hoc test was used to compare groups in (D and E). *$p < 0.05$; ***$p < 0.001$; ****$p < 0.0001$; n.s. = not significant.

plasma from Ad-SF7-Fc-vaccinated mice versus Ad-null-vaccinated mice (Figures 3F and 3G). To determine if Ad-SF7-Fc triggers NK and T cell infiltration into CT26 tumors, we performed immunohistochemistry and found a moderate increase in $CD3^+$ T cells and $DX5^+$ NK cells in mice vaccinated with Ad-SF7-Fc/CT26 lysate in comparison with Ad-null (Figure 3H). Since only expression of DX5 was used to identify NK cells, it is possible minor populations of other $DX5^+$ lymphocytes were counted as well. Altogether, this suggests that Ad-SF7-Fc is capable of generating a memory immune response in the CT26 model, but that this response is not humoral in nature, implying that it is cell mediated.

Ad-SF7-Fc controls B16-F10 tumor growth without modulating T cell exhaustion or remodeling the TME

Since we found that Ad-SF7-Fc augments Th1 cytokine/chemokine responses, and because it is known that BALB/c mice have Th2 skewed immune responses,[18] we reasoned that Ad-SF7-Fc may function better in the B16-F10 tumor model in C57BL/6 mice. We first confirmed that our recombinant Ad5 viruses could infect B16 cells (Figure S3A). Assessing the impact of SF7-Fc overexpression in the TME, we found significantly reduced tumor volumes and improved survival in B16 tumors treated with Ad-SF7-Fc in comparison with the Ad-null-treated controls (Figures 4A and 4B). Considering we recently discovered that SLAMF7 signaling on $CD8^+$ T cells reprograms them toward exhaustion,[10] we assessed the exhaustion status of $CD8^+$ tumor-infiltrating lymphocytes (TILs) from B16 tumors. We found no significant changes in the frequency of $Tox^{high}PD\text{-}1^{high}$ exhausted $CD8^+$ TILs, nor any surface markers of T cell exhaustion, or proliferation in Ad-SF7-Fc-treated tumors (Figures 4C–4F and S4A–S4D). Furthermore, we found no changes in the same markers on $CD4^+$ TILs (Figures S4E–S4I). After reconstructing the exhaustion developmental trajectory in $CD8^+$ TILs,[10,19] we found that Ad-SF7-Fc does not impact progression through this trajectory (Figure 4G).

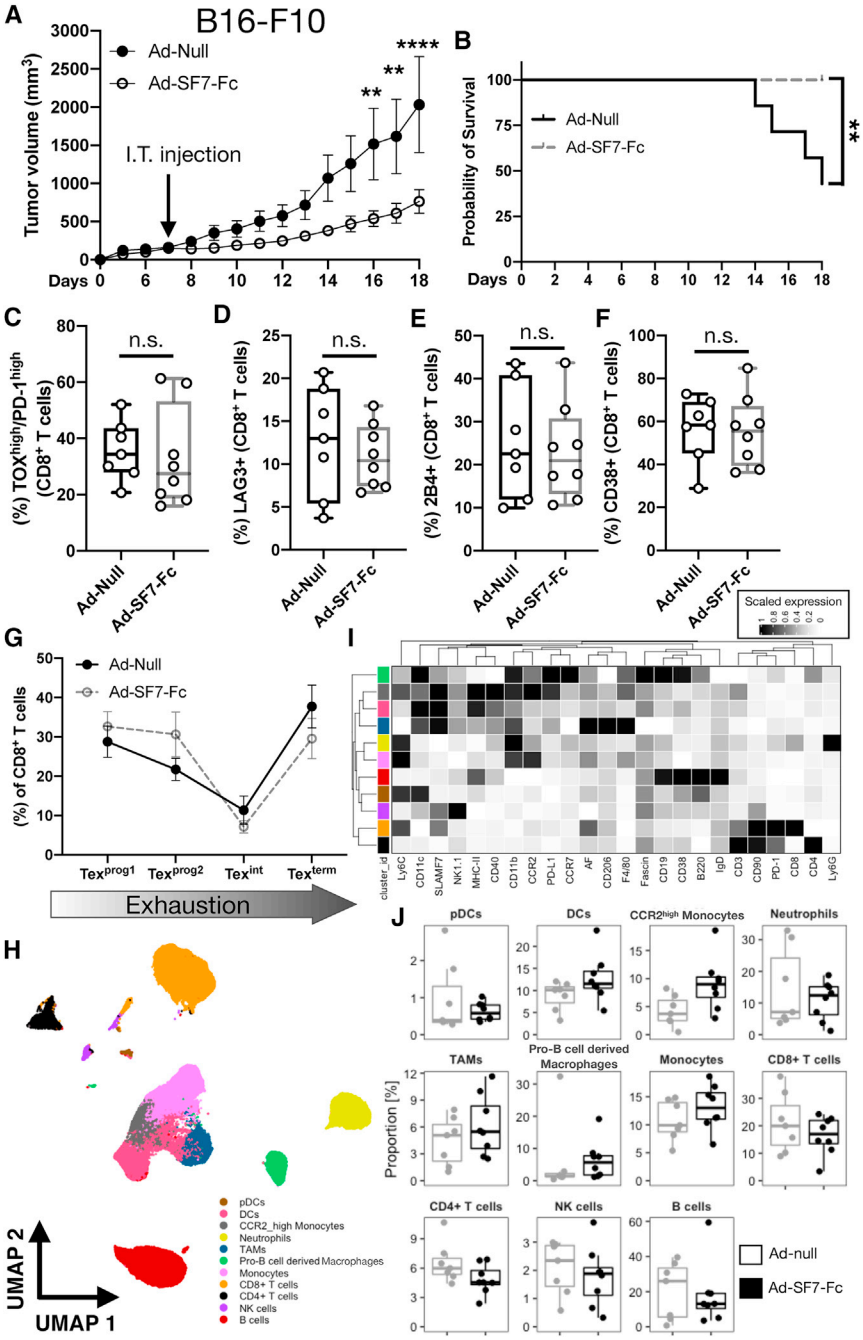

Figure 4. Ad-SF7-Fc controls B16 tumor growth without affecting T cell exhaustion or remodeling the TME

(A) C57BL/6 mice were inoculated with 4×10^5 B16-F10 cells and on day seven were treated I.T. with 1×10^{10} v.p. of either Ad-null or Ad-SF7-Fc. (B) Kaplan-Meier survival curve of virus treated mice. TILs from virus treated B16 tumors were isolated on day 18 and the frequency of $TOX^{high}PD\text{-}1^{high}$ $CD8^+$ T cells (C), LAG3+ $CD8^+$ T cells (D), 2B4+ $CD8^+$ T cells (E), and $CD38^+$ $CD8^+$ T cells (F) was assessed. (G) The exhaustion developmental trajectory (assessed by co-expression of SLAMF6 and CD69)[19] of $CD8^+$ TILs was compared between Ad-null and Ad-SF7-Fc treated tumors. (H) Tumor infiltrating immune cells from Ad-null and Ad-SF7-Fc treated B16 tumors were assessed by high dimensional single-cell spectral cytometry. FlowSOM-generated clusters were displayed on a UMAP dimensionally reduction plot. (I) Marker expression across all clusters in (H). (J) Frequency of each immune cell subset from (H and I) compared across Ad-null and Ad-SF7-Fc-treated B16 tumors. Data in (A and G) presented as mean ± standard error of the mean. The log rank test was used to compare groups in (B). Two-way ANOVA with Tukey's multiple comparison test used to compare groups in (A and G). Unpaired, two-tailed t test used to compare groups in (C–F). A generalized linear mixed model was used to compare groups in (J). All data representative of two independent experiments showing similar results. **p < 0.01; ****p < 0.0001; n.s. not significant. AF = autofluorescence.

We also profiled the immune TME of these mice using high dimensional single-cell spectral cytometry. Unbiased clustering revealed 11 distinct immune cell subsets (Figure 4H), each displaying expected marker expression patterns (Figure 4I). The frequency of each cell subset did not significantly change between Ad-SF7-Fc-treated and Ad-null-treated B16 tumors (Figure 4J), suggesting that Ad-SF7-Fc does not globally remodel the TME.

SLAMF7 expression across the TME and tumor-infiltrating myeloid cell phenotypes in Ad-SF7-Fc-treated mice

We next wanted to identify which cell types in the TME express SLAMF7, and thus might be modulated by our Ad-SF7-Fc vector. Using B16 tumor-bearing SLAMF7-deficient ($SLAMF7^{-/-}$) mice treated with Ad-null, we determined SLAMF7 expression across the TME (Figure 5A). Because we previously found that Ad-SF7-Fc was able to induce DC activation (Figure 1D) and IL-12 production (Figures 2A and 2B), we wished to further investigate tumor-infiltrating DC phenotypes in our B16 model. We identified seven distinct DC subsets (Figures 5B and 5C). We also included markers in our panel allowing the identification of the recently described mature regulatory dendritic cell (mregDC) subset[20] and found that our panel was capable of efficiently identifying mature regulatory dendritic cells in an unbiased manner (Figures 5B, 5C, and S5A). Additionally, we identified high co-expression of SLAMF7 and CD38 on the DC1 B subset (Figure 5D), which was intriguing, because we recently identified a pathogenic subset of Tumor-associated macrophages (TAMs) in clear cell renal cell carcinoma (ccRCC) co-expressing the same markers.[10] Through a

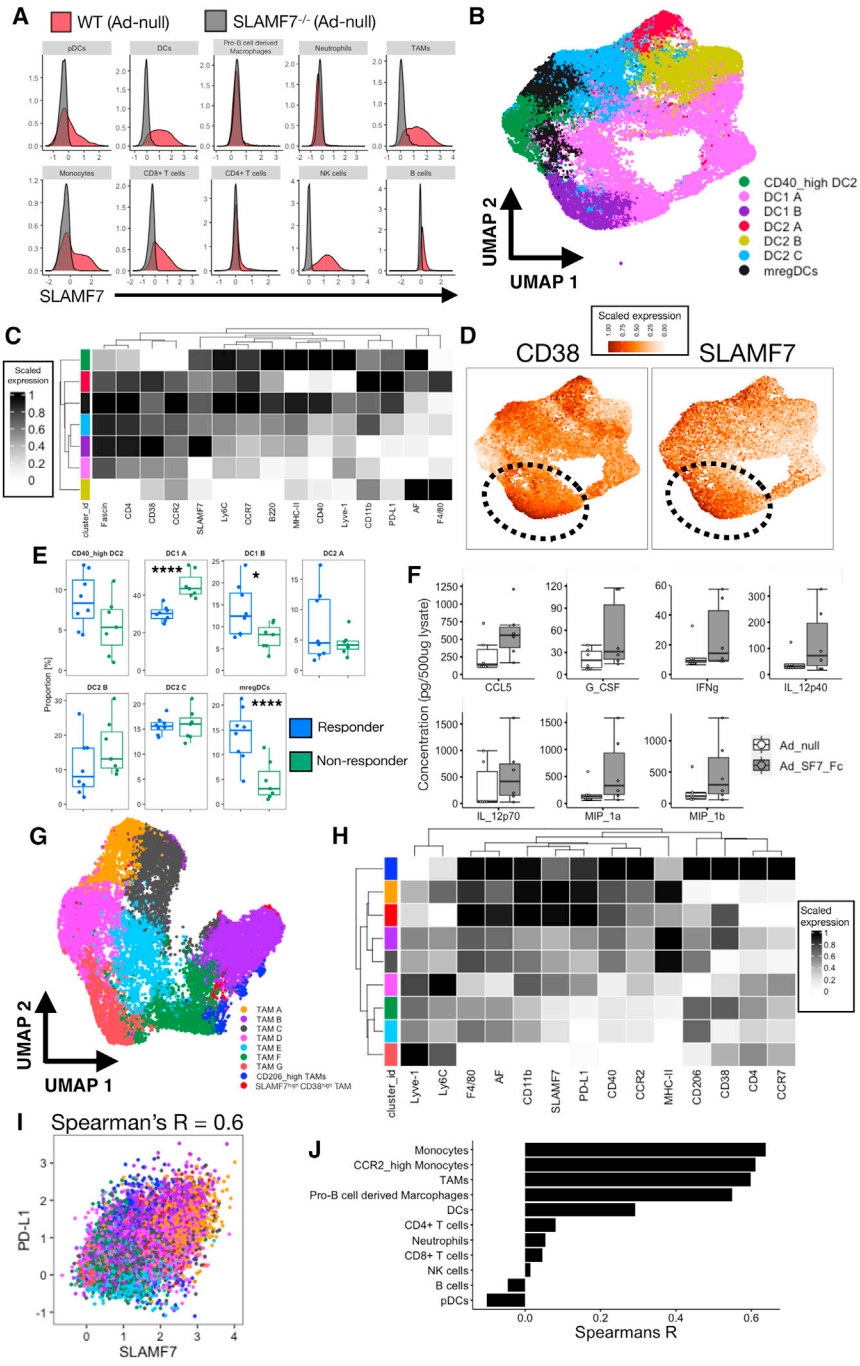

Figure 5. SLAMF7 expression across the TME and tumor inflating myeloid cell phenotypes following Ad-SF7-Fc treatment

(A) SLAMF7 expression across immune cell subsets in B16 tumors after Ad-null treatment. (B) DC subsets in tumors treated with either Ad-null or Ad-SF7-Fc clustered with FlowSOM and displayed with UMAP. (C) Marker expression from clusters in (B). (D) CD38 and SLAMF7 expression displayed on UMAP plot of DCs from (B). (E) Frequency of DC subsets between mice whose B16 tumors respond to I.T. adenovirus treatment or not. (F) Cytokine and chemokine expression from Ad-null and Ad-SF7-Fc treated B16 tumors. (G) TAM subsets in tumors treated with either Ad-null or Ad-SF7-Fc clustered with FlowSOM and displayed with UMAP. (H) Marker expression from clusters in (G). (I) Co-expression of SLAMF7 and PD-L1 on all TAMs (colored by subset). (J) Spearman's correlation coefficient of SLAMF7 and PD-L1 on all immune cell subsets from B16 tumors treated with adenovirus. A generalized linear mixed model was used to compare groups in (E). An unpaired, two-tailed t test used to compare groups in (F). All data representative of two independent experiments showing similar results. AF = autofluorescence.

comparison of frequencies of DC subsets across Ad-SF7-Fc-treated mice responding or not responding to treatment, we noted that responding mice had more of the DC1 B subset, suggesting that, in contrast to TAMs, DCs co-expressing these markers might be anti-tumorigenic (Figure 5E). This is not surprising; DCs are known to express EAT-2,[21] suggesting that SLAMF7 activation in these cells induces IL-12 and pro-inflammatory responses. Supporting this, we found higher expression of IL-12 and other pro-inflammatory cytokines in the tumors of Ad-SF7-Fc treated B16 tumors in comparison to Ad-null (Figure 5F).

We investigated TAM heterogeneity in our model and identified nine TAM subsets (Figures 5G and 5H). We found a SLAMF7^{high}CD38^{high} TAM subset similar to the one we previously identified in patients with ccRCC,[10] suggesting this subset may be conserved across tumors and species (Figures 5G and 5H). However, Ad-SF7-Fc treatment did not alter the frequency of this subset (Figure S5C). Interestingly, we found that TAM subsets expressing SLAMF7 also co-expressed programmed death ligand 1 (PD-L1), with a correlation of 0.6 (Figures 5I and S5B). We extended this analysis across the TME and found it to be conserved across myeloid cells, except for pDCs and neutrophils (Figure 5J).[8]

EAT-2 expression in tumor-infiltrating innate immune cells identifies mice able to control B16 tumors

As the presence of EAT-2 determines whether SLAMF7 functions as an activating or inhibitory receptor,[11] we examined EAT-2 expression in tumor-infiltrating immune cells in our B16 model. While we found that treatment with Ad-SF7-Fc did not change EAT-2 levels in NK cells or DCs in comparison with Ad-null (data not shown), we found that B16 tumors responding to adenovirus treatment had significantly higher expression of EAT-2 in NK cells (Figure 6A), cDC2 cells (Figure 6B), and cDC1 cells (Figure 6C). To determine if increased EAT-2 expression controls tumor growth, we treated CT26 tumors I.T. with our previously described

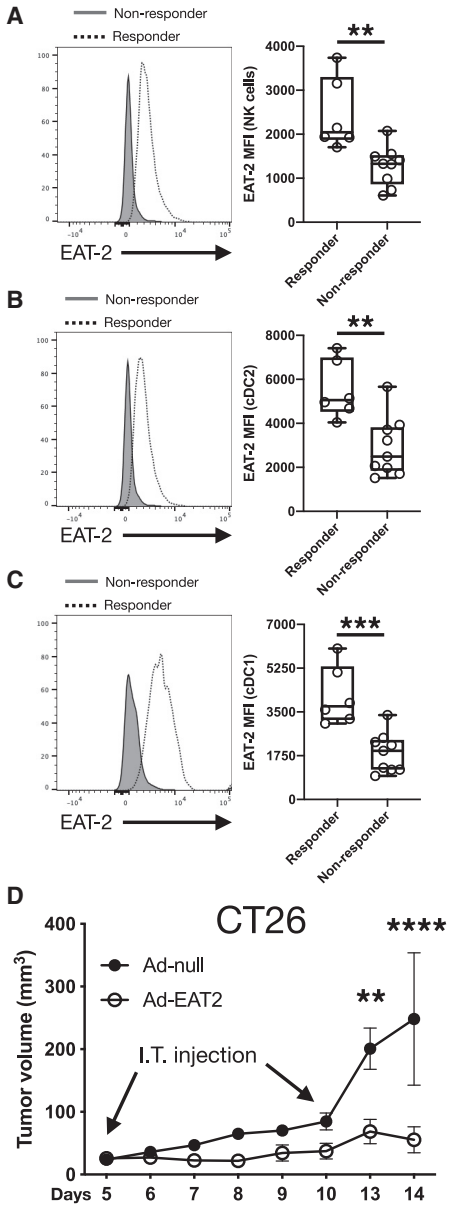

Figure 6. EAT-2 expression in immune cells from adenovirus treated B16 tumors as an indicator of response to treatment

(A) Expression of EAT-2 in B16 tumor-infiltrating NK cells from tumors treated with adenovirus. (B) Expression of EAT-2 in B16 tumor-infiltrating cDC2 cells from tumors treated with adenovirus. (C) Expression of EAT-2 in B16 tumor-infiltrating cDC1 cells from tumors treated with adenovirus. (D) Tumor volumes of CT26 tumors treated I.T. twice with 1×10^{10} v.p. of either Ad-null or Ad-EAT-2. All data are presented as mean ± standard error of the mean and representative of a single experiment. Two-way ANOVA with Tukey's multiple comparison test used to compare groups in (D). An unpaired, two-tailed t test was used to compare groups in (A–C). **p < 0.01; ***p < 0.001; ****p < 0.0001.

EAT-2-expressing adenovirus vector.[22] We discovered that Ad-EAT-2-treated CT26 tumors displayed superior tumor control compared with Ad-null-treated tumors (Figure 6D). These findings suggest that modulating SLAMF7 signaling via EAT-2 enhances the pro-inflammatory activity of tumor-infiltrating innate immune cells, and thus results in better tumor control.

Cell type-specific, single-cell predictions of the function of Ad-SF7-Fc *in vivo*

Because SLAMF7 is a homotypic receptor, and since SF7-Fc is composed of the extracellular domain of SLAMF7, SF7-Fc can conceivably function to both activate and/or block SLAMF7 signaling, depending on local environmental factors and the cell type in question. Additionally, activating or blocking SLAMF7 can have vastly different outcomes on different cell types depending on the presence of EAT-2,[9,11] which may mechanistically explain how Ad-SF7-Fc achieves tumor control. Therefore, we devised an approach using high dimensional spectral cytometry, which allowed us to predict if SF7-Fc was activating or blocking SLAMF7 at the single-cell level (Figure 7A; see materials and methods). We found that Ad-SF7-Fc was primarily activating DCs and monocytes, having equally opposing effects on TAMs and $CD8^+$ T cells, and primarily blocking pDCs and NK cells (Figures 7B–7F, S6C, and S6D). We next calculated the ratio of SLAMF7 activation versus blocking on each cell type between mice responding to Ad-SF7-Fc or not, and found that responding mice had considerably more pDC activation (Figure 7G).

Alterations in the immune TME in SLAMF7$^{-/-}$ mice

We also compared immune cell subsets between Ad-null-treated wild-type (WT) and Ad-null-treated SLAMF7$^{-/-}$ mice used for prediction analyses. We detected decreased levels of NK and $CD8^+$ T cells in the TME of SLAMF7$^{-/-}$ mice (Figure S6E); the latter is consistent with our previous work.[10] We also investigated TAM subsets in these mice and found a dramatic re-structuring of the TAM landscape in SLAMF7$^{-/-}$ mice (Figures S6F and S6G). Finally, we identified all markers on all cell subsets statistically different between WT and SLAMF7$^{-/-}$ mice and found decreased PD-1 and increased PD-L1 on NK cells (Figure 7H). Together, these findings highlight the broad and diverse roles of SLAMF7 signaling in the TME.

Immunological elastic net identifies features underlying tumor response to Ad-SF7-Fc

To determine why some tumors respond with an attenuation of growth to Ad-SF7-Fc and others do not, we employed a machine learning-based approach using the recently described immunological elastic net (iEN) algorithm.[23] Into iEN, we input multiple datasets representing a host of systemic and tumor-localized immune measurements, and a table of immune-specific priors (Figure 8A and Table S1; see materials and methods). We validated that our iEN model can discriminate responders from non-responders, and that the addition of our priors improves model performance (Figures 8B and 8C). To determine the factors allowing iEN to identify responders, we generated and performed a network analysis (See materials and methods), which showed clustering of common immune archetypes (Figure 8D). Coloring features on the network by those which were increased or decreased in responding B16

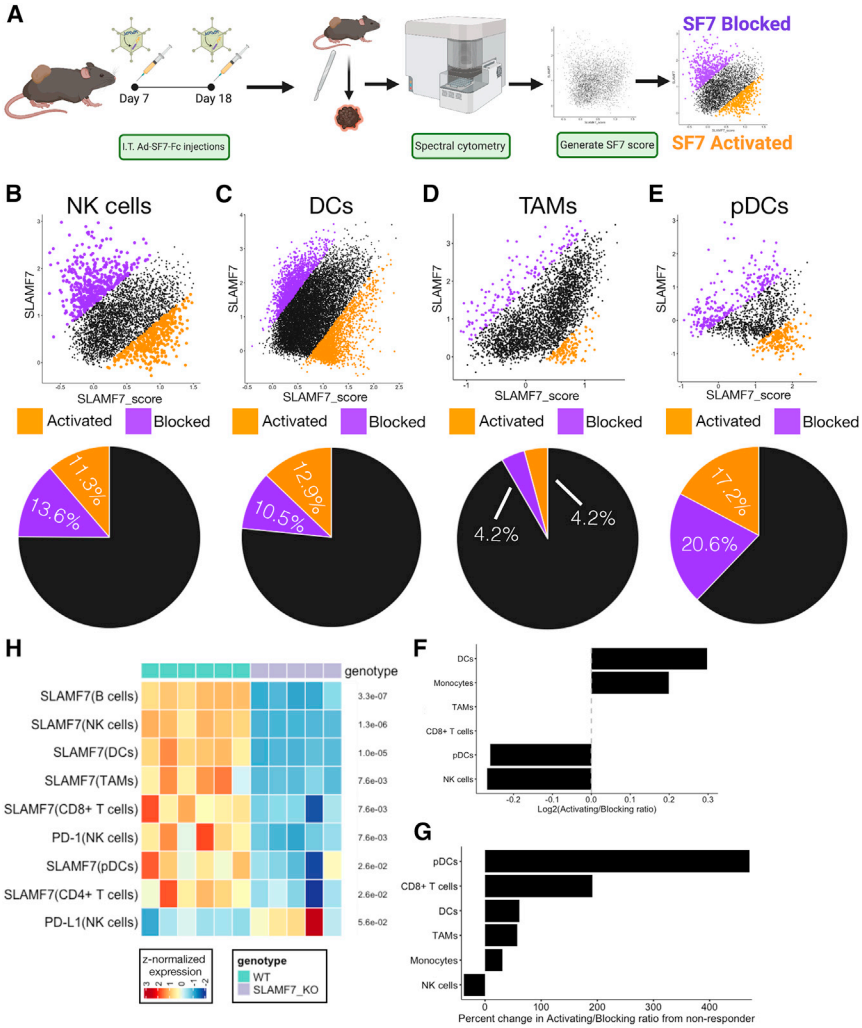

Figure 7. Mechanistic predictions of the function of SF7-Fc in B16 tumors

(A) Schematic overview of experimental design. (B) Dot plot of SLAMF7 and SLAMF7_score for NK cells (See materials and methods), with cells predicted to have their SLAMF7 receptor activated colored orange and cells predicted to have their receptor blocked colored purple. Pie charts under each dot plot display frequency of predictions. (C) Same as (B), but for DCs. (D) Same as (B), but for TAMs. (E) Same as (B), but for pDCs. (F) Log_2 transformed ratio of frequency of SLAMF7 activation to blocking for each cell type in the TME with SLAMF7 expression. (G) Percent change in the ratio of predicted SLAMF7 activation to blocking between B16 tumors responding to Ad-SF7-Fc and not responding, plotted for each cell type. (H) Heatmap of differential marker expression across B16 tumor-infiltrating immune cell subsets in Ad-null treated WT and SLAMF7$^{-/-}$ mice. The p value was adjusted for multiple comparisons displayed on right of each row. Only markers below an FDR of 0.6 are displayed.

tumors, we found many expected changes in responding tumors like: increased CD8$^+$ T cells, more Tex^{prog1} CD8$^+$ T cells,[19] increased intra-tumoral IFNγ,[24] fewer neutrophils (myeloid-derived suppressor cells),[25] fewer TAMs, and less CD206 expression on TAMs (Figure 8E and Table S2).[26,27] Critically, we found a number of features supporting the ability of SLAMF7 signaling to modulate tumor control, buttressing our hypothesis that Ad-SF7-Fc functions to control tumor growth via DC and innate immune cell stimulation. The iEN found increased levels of IL-12(p40) in responding tumors and increased SLAMF7 on TAMs and DCs from responding tumors (Figure 8E and Table S2). iEN also found that higher predicted activation of SLAMF7 on TAMs was important in separating responders that, paired with our earlier data showing high co-expression of SLAMF7 and PD-L1 on TAMs, suggests that SLAMF7 may be able to modulate this immune suppressive pathway to achieve tumor control (Figure 8E and Table S2). It should be noted that our model generated by iEN is specific to our experimental setup and is not generalizable across tumor models or other therapeutic modalities.

DISCUSSION

Our findings demonstrate that modulation of SLAMF7 signaling in the TME induces beneficial anti-tumor responses. Specifically, the ability of Ad-SF7-Fc to induce IL-12 production, putatively by DC activation, is supported by previous findings that in myeloid cells lacking EAT-2, SLAMF7 activation inhibits IL-12 production.[13] As DCs are known to express EAT-2,[21] it is to be expected that SLAMF7 activation in these cells should allow for IL-12 production. Due to the well-known importance of IL-12 in inducing anti-tumor immune responses,[28] SLAMF7 modulation of this pathway is likely one mechanism by which Ad-SF7-Fc achieves tumor control. Complementing this IL-12 response is the induction of type I IFN by Ad-SF7-Fc. Type I IFN responses can be beneficial in tumor control and achieve this via multiple mechanisms.[29,30] Indeed, previous studies have found that IL-12 and type I IFNs can synergize to induce potent immune activation,[31] and there is much interest in combination cancer immunotherapies involving IL-12.[32] Since pDCs are one of the primary producers of type I IFNs,[33] express SLAMF7 in the TME, and express EAT-2 (www.immgen.org), it is plausible that SLAMF7 activation on intratumoral pDCs drives pDC production of type I IFNs.

Our discovery that Ad-SF7-Fc does not modulate T cell exhaustion in the TME or significantly increase humoral immune responses against tumors was unexpected based on our previous work.[10,14] However, there are a number of explanations for this, including the use of an adenoviral vector to deliver SF7-Fc, contributions from the TME itself, and the potential for SF7-Fc to both block and activate SLAMF7 simultaneously. The latter we worked to address using our novel

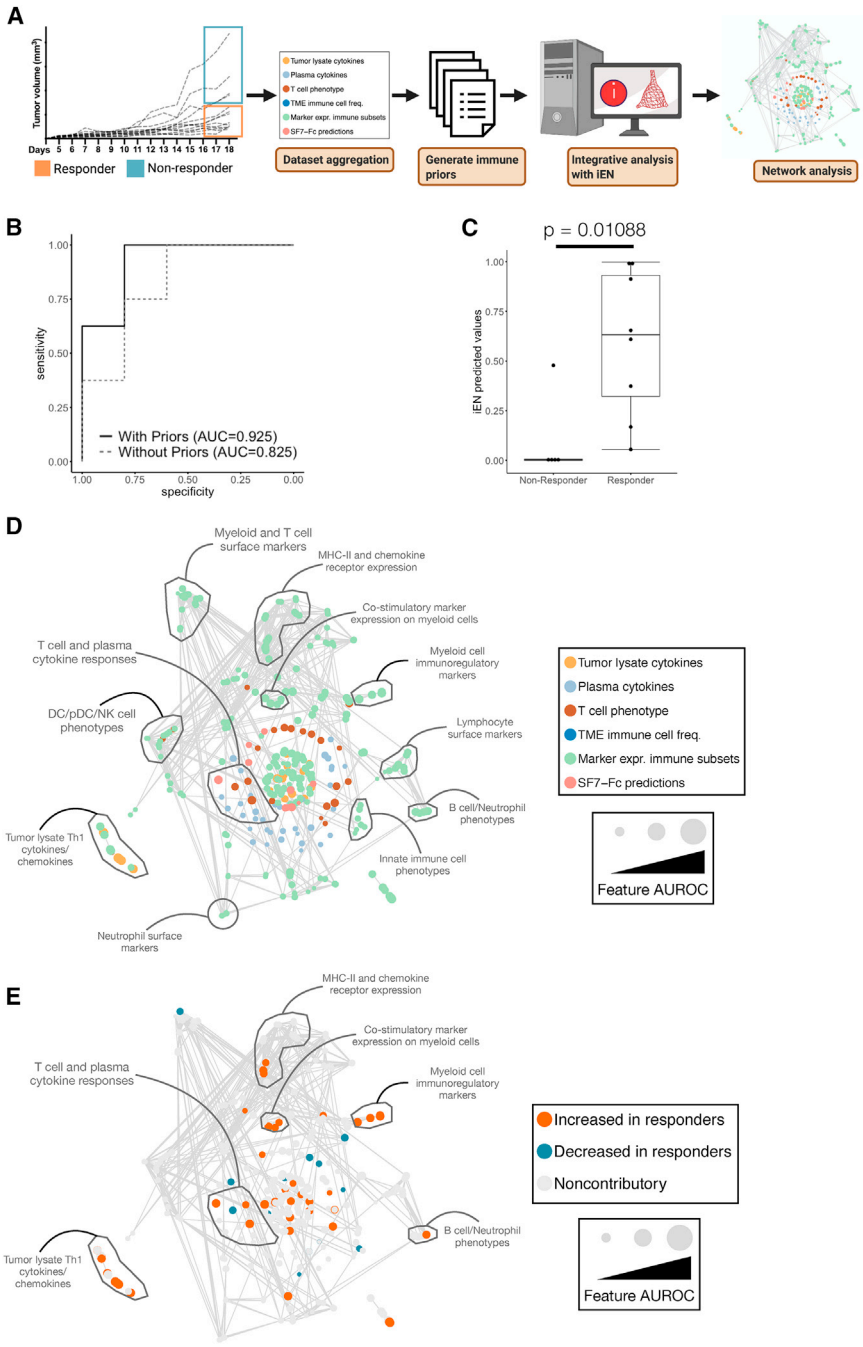

Figure 8. iEN machine learning identifies factors underlying tumor response to Ad-SF7-Fc

(A) Schematic overview of experimental design. (B) The receiver operating curve (ROC) of iEN model performance with and without inclusion of priors. (C) Comparison of iEN predicted values (arbitrary units) between responders, with statistical comparison performed with Wilcoxon sum rank test. (D) The iEN model network where each node is a feature entered into the model and is scaled by its individual area under the ROC (AUROC). Edges are significant spearman correlations between features ($p < 0.05$) after Bonferroni correction for multiple comparisons. Nodes are colored by the dataset they originate from and communities of shared immunological archetypes are highlighted. (E) The same network from (D), but with nodes colored by iEN model coefficients identifying features increased or decreased in responders and which contributed to model performance. Noncontributory features have a 0 iEN model coefficient. Data analyzed and presented are aggregated from two independent B16 tumor experiments.

in vivo prediction approach, which yielded results consistent with our other studies showing that SF7-Fc activates DCs. Our approach also found that B16 tumors responding to Ad-SF7-Fc had more SLAMF7 activation on pDCs, which corresponds with increased type I IFN production by Ad-SF7-Fc. Since Ad-SF7-Fc does seem to both activate and block SLAMF7 on the same cell subsets, our results suggest that targeting SLAMF7 modulation to particular immune cell types could prove more effective. Importantly, while our results showing Ad-SF7-Fc can induce an abscopal effect (presumably via induction of an adaptive immune response), and that this effect is likely due to augmentation of cell-mediated immunity (T cell responses), we did not directly investigate this and only ruled out augmentation of the humoral arm of the adaptive immune response.

Our studies using SLAMF7$^{-/-}$ mice have yielded a number of insights into the role of SLAMF7 in the TME. Among these is the decreased frequency of NK and CD8^{+} T cells in the TME of SLAMF7$^{-/-}$ mice, which is consistent with our previous work.[10] This finding provides evidence that SLAMF7 may function as an adhesion molecule important for lymphocyte egress and residency in the TME. Discovering that tumor-infiltrating NK cells from SLAMF7$^{-/-}$ mice do not express PD-1 in contrast to WT mice is particularly interesting given that we recently found SLAMF7 signaling on T cells is able to modulate PD-1 expression.[10] This suggests a similar mechanism may be present in NK cells and may contribute to tumor control as PD-1 signaling is inhibitory on NK cells.[34] Analogously, we found increased PD-L1 expression on NK cells from SLAMF7$^{-/-}$ mice, supporting potentially linked roles for SLAMF7 in the regulation of PD-1/PD-L1 receptor pair.

Perhaps our most interesting observation was the strong co-expression of SLAMF7 and PD-L1 on tumor-infiltrating myeloid cells that we observed. Of the myeloid cell types expressing SLAMF7,

DCs had the lowest co-expression of SLAMF7 with PD-L1, which may be due to the fact that these cells express EAT-2, whereas the other subsets do not.[21] The high co-expression of these two markers may also explain our previous findings that a subset of SLAMF7^{high}CD38^{high} TAMs was linked to poor survival in ccRCC, since these cells have higher PD-L1 expression than other TAM subsets (data not shown).[10,35] The theory that SLAMF7 may be able to modulate PD-L1 expression on TAMs (or other myeloid cell types) is supported by results from our machine learning analysis of responses to Ad-SF7-Fc. Here, we found that responders counterintuitively had higher expression of PD-L1 on TAMs, but also had more SLAMF7 on TAMs and critically, more predicted SLAMF7 activation on TAMs. Taken together, this implies that either modulation of SLAMF7 with SF7-Fc induces anti-tumor responses in TAMs, or the strong innate immune response of Ad-SF7-Fc is capable of overcoming coincidentally induced pro-tumor TAM responses.

By combining modulation of SLAMF7 signaling with delivery and immune stimulation via a recombinant adenovirus vector, we provide proof-of-concept that such an approach can achieve superior tumor control compared with an empty viral vector. While our approach functions primarily by augmentation of the innate immune system, future derivations of this paradigm capable of inducing pan-adaptive immune responses should prove highly effective as a cancer immunotherapeutic strategy.

MATERIALS AND METHODS

Adenovirus vector construction

All adenovirus used in this study are of human serotype 5. Ad-null was constructed and purified as previously described.[36] Ad-SF7-Fc was constructed and purified in a similar manner, where the SLAMF7 extracellular domain fused to mIgG1-Fc (SLAMF7/mIgG-Fc) (NCBI Reference Sequence: NM_144539.5) was excised using primers flanked by *EcoRI* and *HindIII* restriction endonucleases (NEB) from a plasmid (Biomatik) and sub-cloned into the pShuttle vector, containing a CMV expression cassette. The resulting pShuttle-SF7-Fc plasmid was linearized with *PmeI* restriction enzyme and homologously recombined with the pAdEasyI Ad vector genome yielding Ad-SF7-Fc. HEK293 cells were transfected with *PacI* linearized plasmid and viable virus was obtained and amplified after several rounds of expanding infection. Ad-SF7-Fc virus was purified using a $CsCl_2$ gradient. The number of viral particles was quantified using optical density measurement at 260 nm, as previously described.[14] All viruses were found to be replication incompetent (RCA free) by both RCA polymerase chain reaction (PCR) (E1 region amplification) and direct sequencing methods, as described previously.[14,22]

Tumor models

All animal procedures were approved by the Michigan State University Institutional Animal Care and Use Committee (http://iacuc.msu.edu/). SLAMF7$^{-/-}$ mice were generated as previously described.[10] CT26 model: 8-week-old male BALB/c mice were injected subcutaneously (S.Q.) in the flank with 1.5×10^5 CT26.CL25 (ATCC, CRL-2639) cells in 100 μL of phosphate-buffered saline (PBS). Eight days later, once visible tumors formed, mice were split randomly into three groups and were either injected I.T. with 10^{10} viral particles (v.p.) of Ad-null (n = 15), Ad-SF7-Fc (n = 15), or not injected (n = 14). Mice were monitored every 2 to 3 days and their tumor size was assessed with calipers. Tumor size was calculated with the following formula: $0.5 \times (\text{Length} \times \text{Width}^2)$. In studies where tumors were placed on both hind flanks, one-half as many cells were injected into each flank at the same time. Mice where a tumor never formed were not included in analysis. B16-F10 model: 4×10^5 B16 tumor cells were injected into the hind flanks of 8- to 12-week-old male C57BL/6J mice as previously described.[10] At day 7 after tumor implantation I.T. injection of Ad-null or Ad-SF7-Fc (n = 7-12 per treatment) was performed using 10^{10} v.p. of respective virus.

Cell culture

CT26 and B16-F10 tumor cell lines were cultured in modified RPMI-1640 media (ATCC, 30-2001) supplemented with 10% heat inactivated fetal bovine serum (FBS), and 1× penicillin, streptomycin and fungizone (PSF) (Invitrogen). HEK-293C7 cells were cultured in DMEM media, supplemented with 10% FBS, 1× PSF, and hygromycin.

ADCC assays were performed as described previously.[37] Briefly, CFSE-stained CT26 cells were plated at 1×10^5 cells/well in U-bottom 96-well cell culture plates. Total splenocytes from naive mice were incubated with CFSE-CT26 cells (20:1 Effector:Target) and cultured for 18 h in presence of plasma (1:200 dilution) from Ad-null/CT26 lysate, Ad-SF7-Fc/CT26 lysate vaccinated, or non-vaccinated mice. Alternatively they were cultured with Dx5+ NK cells isolated via magnetic beads (Miltenyi kit: 130-052-501) from naive mice and incubated with CFSE-CT26 cells (1:1 E:T ratio) overnight in presence of plasma (1:50 dilution) from vaccinated mice. Cultures contained 2 ng/mL of murine IL-2 (R&D). Trypsinized cells were stained with a viability dye and analyzed by flow cytometry on a BD LSR II cytometer.

Vaccination studies

Six-week-old BALB/c male mice were injected twice intramuscularly (n = 6) over a period of 1 month (days 0 and 12) with 200 μg of CT26 tumor lysate, tumor lysate + 10^{10} v.p./mouse of Ad-null, tumor lysate + 10^{10} v.p./mouse of Ad-SF7-Fc, or not injected (naive, n = 4). On day 27, mice were sacrificed, tumors were harvested, and immunohistochemistry (IHC) was performed.

Tumor lysate preparation

Tumor lysates were prepared using five freeze-thaw cycles, followed by sonication and centrifugation as described previously.[38] Sample concentration was determined using BCA protein kit (Sigma-Aldrich) per manufacturer's protocol and as previously described,[39] after which the samples were stored at −80°C until use.

Innate immune study

Six-week-old BALB/c male mice were injected I.V. with 10^{10} v.p. of Ad-null (n = 6), Ad-SF7-Fc (n = 6), or not injected, naive (n = 3).

After 10 h, plasma and spleens were collected for Bioplex and flow cytometry analysis.

Flow cytometry and spectral cytometry

Cells were prepared and stained as previously described.[10] All antibodies used are listed in (Table S3). Intracellular staining was performed with the Cytofix/Perm kit (BD Biosciences) per the manufacturer's instructions. Viability staining was performed with Zombie NIR Fixable Viability dye (BioLegend). Fc receptors were blocked in all samples during staining with mouse Fc block (BD Biosciences). When staining cells from B16 tumors, BD Brilliant Stain buffer (cat: 563794) was used per the manufacturer's instruction. Samples were acquired on either a five-laser Cytek Aurora Spectral Cytometer or a three-laser BD LSR II cytometer and data were analyzed using FlowJo version 10.6.1 (Tree Star) and/or R. All gating schemes can be found in (Figure S2). High dimensional single-cell spectral cytometry was performed in R by first cleaning up the data in FlowJo (Figure S2). Data were exported from FlowJo as FCS files, which were then loaded into R. The CATALYST package was used to perform all analyses with a cell annotation and dimensionality reduction approach as previously described.[10,40] An arcsinh transformation of 6000 was used for all spectral cytometry data. Analysis was performed on cells pooled from all conditions as previously described.[40]

Cytokine and chemokine analysis

Mouse 23-analyte multiplex-based assay was used to determine cytokine/chemokine concentrations via Luminex 100 per manufacturer's protocol (Bio-Rad), as previously described.[8,14] Plasma was used at 1:4 dilution and 500 μg of tumor lysate was assessed.

ELISA analysis

Six-week-old BALB/c male mice were given three doses of 200 μg of CT26 tumor lysate and 10^{10} v.p. of Ad-null or Ad-SF7-Fc intraperitoneally over a period of 5 weeks, at which point they were injected with 2.5×10^5 CT26 tumor cells. At 41 days after the tumor challenge, plasma from Ad-null (n = 6), Ad-SF7-Fc (n = 7), and naive (n = 2) mice was collected. ELISA assessing levels of CT26-specific antibodies in the plasma was assessed as described previously,[41] where 100 μg of CT26 lysate was plated per well in a high-binding 96-well flat-bottom plate (Corning), incubated at 4°C overnight, and plasma was plated at 1:100, 1:200, and 1:500 dilutions.

Quantitative RT-PCR

Six-week-old BALB/c male mice were injected I.V. with 10^{10} v.p. of Ad-null (n = 6), Ad-SF7-Fc (n = 6) or not injected, naive (n = 3). 6 h later, spleens were harvested and snap frozen in liquid nitrogen. RNA was extracted using Trizol reagent (Life Technologies), per manufacturer's protocol. cDNA was generated using SuperStrand First Strand Synthesis Kit III (Invitrogen) from Trizol-isolated RNA per the manufacturer's protocol. Quantitative RT-PCR was performed using SYBR green PCR Mastermix (Life Technologies) and analyzed on a QuantStudio7 system (Thermofisher). The following primers were used: *Isg15*: For: 5′GGTGTCCGTGACTAACTCCAT-3′, Rev: 5'TGGAAAGGGTAAGACCGTCCT'3; *Oas2*: For: 5′TTGAAGAGGAATACATGCGGAAG-3′, Rev: 5′GGGTCTGCATTACTGGCACTT-3′; *Ifna*: For: 5′GCCTTGACACTCCTGGTACAAATGAG-3′, Rev: 5′CAGCACATTGGCAGAGGAAGACAG-3′; *Ifnb*: For: 5′TGGGTGGAATGAGACTATTGTTG-3′, Rev: 5′CTCCCACGTCAATCTTTCCTC-3′; *Il6*: For: 5′TAGTCCTTCCTACCCCAATTTCC-3′, Rev: 5′TTGGTCCTTAGCCACTCCTTC-3′; *Il12*: For: 5′TGGTTTGCCATCGTTTTGCTG-3′, Rev: 5′ACAGAGGTTCACTGTTTCT-3′; *csf2*: For: 5′GGCCTTGGAAGCATGTAGAGG-3′, Rev: 5′GGAGAACTCGTTAGAGACGACTT-3′; *mGapdh*: For: 3′AGAACATCATCCCTGCATCC3′, Rev: 5′CACATTGGGGGTAGGAACAC-3′.

HEK-293-C7 cells were plated at $2x10^6$ cells/mL in 12-well plates in 500 μL of complete RPMI media. Ad-null and Ad-SF7-Fc viruses were added at multiplicity of infection (MOI) of 10^4 v.p./cell. Mock treated cells were treated with PBS. After 12 h, RNA was extracted using Trizol. Primers used: *Slamf7*: For: 5′GGCACATGCGTGATCAATCT-3′, Rev: 5′ATCGCCAAGCGATACTCAGA-3′; *hGAPDH*: For: 5′GGGTGTGAACCATGAGAAGTATGAC-3′, Rev: 5′GCCATCCACAGTCTTCTGGGT-3′. The $\Delta\Delta C_t$ method was used to compare gene expression across conditions and all genes were normalized to *GAPDH* in all experiments.

Immunohistochemistry

Samples were fixed in 10% neutral buffered formalin, embedded in paraffin, and sectioned on a rotary microtome at 4 μm. Sections were placed on positively charged slides and dried at 56°C overnight. After deparaffinization in Xylene, slides underwent heat-induced epitope retrieval in a steamer using Scytek Citrate Plus Retrieval pH 6.0 followed by several rinses in distilled water. Endogenous Peroxidase was blocked via a 3% Hydrogen Peroxide/Methanol bath for 30 min. After blocking for non-specific protein with Rodent Block M (Biocare) for 10 or 20 min, sections were incubated with appropriate primary antibodies as described in (Table S4). Micro-Polymer (Biocare) reagents were subsequently applied for specified incubations followed by reaction development with Romulin AEC (Biocare) and counterstained with cat hematoxylin. The number of positive cells was manually counted under magnification 10× for CD3-stained, 20× for CD8-stained, and 40× for DX5-stained slides, where five areas per sample, and at least two sections per sample were used.

Intra-tumor immune cell isolation

Tumors were surgically removed from mice and placed in ice-cold PBS. Tumors were minced and non-tumor tissue was removed. Cell suspension was pelleted and resuspended in RPMI with 0.5 mg/mL Collagenase IV (Millipore-Sigma) and 1×10^3 IU/mL DNaseI (Millipore-Sigma) under constant, gentle agitation at 37°C for 1 h. Digestion was stopped with EDTA and RPMI-1640 supplemented with 10% FBS and cell suspension was filtered through a 40μm cell strainer. Cells were then subject to a Ficoll-Plaque gradient centrifugation step to enrich for immune cells.

SLAMF7 activating and blocking predictions

24 h after a second I.T. injection of Ad-null or Ad-SF7-Fc, the tumors were harvested, cells were stained, and analyzed on a Cytek Aurora spectral cytometer, all as described above. We also confirmed that acute administration of adenovirus does not remodel the TME (Figure S6B). Cells were clustered and annotated as described above. To perform predictions, first we obtained a signature for what a cell with SLAMF7 signaling looks like. To get this, we first subseted to just a single immune cell type, calculated the median expression of each marker in that cell type in WT (Ad-null treated) and SLAMF7$^{-/-}$ (Ad-null treated), and subtract the SLAMF7$^{-/-}$ marker expression values from WT. We then selected the markers with the most positive and most negative difference to use as a signature. This was done via manual inspection and typically the top three to four and bottom four to five markers were chosen. Markers that would never be expected to be expressed on a particular cell type were excluded. This yielded a SLAMF7 signature of both up-regulated and down-regulated markers on a cell-type-specific basis.

We then subseted the same cell type from WT (Ad-SF7-Fc treated) mice and used the previously calculated signature to generate a SLAMF7_score for each cell. The score was calculated using a previously published formula used to obtain signature scores from scRNA-seq data.[42] Importantly, our prior work demonstrated that activation of SLAMF7 with SF7-Fc leads to its down-regulation,[8] and we confirmed that blocking SLAMF7 with SF7-Fc leads to its up-regulation (Figure S6A).[8] Therefore, for each cell type we plotted the SLAMF7_score by SLAMF7 expression as a dot plot and expected that cells where SLAMF7 is being blocked should have high SLAMF7 expression (Figure S6A) and a low SLAMF7_score, while cells where SLAMF7 is being activated should have low SLAMF7 expression[8] and a high SLAMF7_score. Cells where SLAMF7 is being activated or inhibited naturally come off the diagonals so we selected the cells at either extreme of the appropriate diagonals as being blocked or activated.

To calculate outliers in an unbiased manner we identified the points on the plot representing the intersection of the 25th percentile of SLAMF7 expression and the 75th percentile of SLAMF7_score for defining the boundary of cells getting SLAMF7 blocked. We did the reverse for cells getting SLAMF7 activated. We now calculate the slope of the diagonal lines passing through each point with a linear model where the *y*-intercept for each line is the model coefficient. To identify the points on either extreme of these lines, we calculated and used the corresponding residuals. This approach was performed only for cell types with considerable levels of SLAMF7 expression (i.e., not CD4^{+} T cells and B cells, which express SLAMF7 at very low levels).

iEN machine learning analysis of tumor response to Ad-SF7-Fc

We first separated mice inoculated with B16 tumors and treated with Ad-SF7-Fc into those who responded and those who did not based on final tumor volume at time of sacrifice (Figure 8A). Next, we pooled together all immune measurements made on these mice across various assays. We then generated a table containing prior immunological knowledge about known responses to adenovirus vectors[22,43–46] and expected marker expression across different cell types (other immune measurements were not weighted in our priors so as to not bias the algorithm) (Table S1). We input all immune measurements into the iEN algorithm along with our priors and perform 10-fold cross-validation.[23] Model validation was performed by calculating the area under the receiver operating curve. Networks were generated as previously described.[23] Briefly, each node is a feature entered into the iEN model and node sizes are scaled by their individual area under the receiver operating curve. Edges are significant spearman correlations between features ($p < 0.05$) after Bonferroni correction for multiple comparisons. Imbedding in two-dimensional space was performed with t-distributed stochastic neighbor embedding.

Statistical analysis

Data in all graphs are presented as mean ± standard error of the mean. Statistical analyses are listed in all figure legends and were performed in either GraphPad Prism V8 or the R computing environment. Cell subset frequency comparisons and differential marker expression on cell subsets from experiments using high dimensional spectral cytometry were statistically compared with a generalized linear mixed model implemented through the diffcyt R package. All heatmaps were locally scaled. No samples/mice were excluded from any analysis except for one Ad-null treated WT and one Ad-SF7-Fc treated WT mouse from the same B16 tumor growth experiment, where an outlier test identified the tumor volume in each mouse as a statistically significant outlier.

DATA AND CODE AVAILABILITY

Raw data are available from the authors upon reasonable request.

Code used for all computational analyses can be found at: https://github.com/poconnel3/OConnell_et_al_Ad-SF7-Fc_paper_code.

SUPPLEMENTAL INFORMATION

Supplemental information can be found online at https://doi.org/10.1016/j.omto.2021.12.004.

ACKNOWLEDGMENTS

We would like to thank the MSU genomics core for assistance with qRT-PCR and the MSU histology core for sample preparation and immunohistochemistry. We also thank Dr. David L. Carlson for assistance with SF7-Fc prediction analysis and Anthony Culos for assistance analyzing iEN models. The data presented herein were obtained using instrumentation in the MSU Flow Cytometry Core Facility with support of Core staff. The facility is funded through user fees and the financial support of Michigan State University's Office of Research & Innovation, College of Osteopathic Medicine, and College of Human Medicine. Y.A.A. and A.A. hold a patent on the SF7-Fc protein. Y.A.A. was supported by the US National Institute of Health grant (1R21AI122808-01) and the Michigan State University Clinical and Translational Sciences Institute (MSU-CTSI). A.A. is supported by the MSU Foundation and the Osteopathic Heritage Foundation.

P.O. is supported by the John A. Penner Endowed Research Fellowship.

AUTHOR CONTRIBUTIONS

P.O. designed all B16 and some CT26 experiments and Y.P. designed some CT26 experiments. P.O., M.K.B., Y.P., and S.H. performed all experiments. M.K.B. performed all bioplex assays. Y.P. analyzed all data related to CT26 experiments and P.O. analyzed all data related to B16 experiments. C.P.H. manage all cell lines. S.G. and C.P.H. prepared all adenoviruses. S.G. managed all mouse work. Y.A.A. conceptualized Ad-SF7-Fc and Ad-EAT-2 and designed the vectors. A.M.A. performed IHC analysis. P.O. performed all high dimensional single-cell spectral cytometry and analyzed all associated data. P.O. conceptualized and performed all computational analyses. P.O. generated all figures and wrote the manuscript, with input and revisions from all authors. Y.A.A. and A.A. supervised the study and provided funding.

DECLARATION OF INTEREST

The authors declare no conflicts of interest exist.

REFERENCES

1. Murciano-Goroff, Y.R., Warner, A.B., and Wolchok, J.D. (2020). The future of cancer immunotherapy: microenvironment-targeting combinations. Cell Res. *30*, 507–519. https://doi.org/10.1038/s41422-020-0337-2.
2. Waldman, A.D., Fritz, J.M., and Lenardo, M.J. (2020). A guide to cancer immunotherapy: from T cell basic science to clinical practice. Nat. Rev. Immunol. *20*, 651–668. https://doi.org/10.1038/s41577-020-0306-5.
3. Young, A., Quandt, Z., and Bluestone, J.A. (2018). The balancing act between cancer immunity and autoimmunity in response to immunotherapy. Cancer Immunol. Res. *6*, 1445–1452. https://doi.org/10.1158/2326-6066.CIR-18-0487.
4. Barrueto, L., Caminero, F., Cash, L., Makris, C., Lamichhane, P., and Deshmukh, R.R. (2020). Resistance to checkpoint inhibition in cancer immunotherapy. Transl. Oncol. *13*, 100738. https://doi.org/10.1016/j.tranon.2019.12.010.
5. Soldatos, T.G., Dimitrakopoulou-Strauss, A., Larribere, L., Hassel, J.C., and Sachpekidis, C. (2018). Retrospective side effect profiling of the metastatic melanoma combination therapy ipilimumab-nivolumab using adverse event data. Diagnostics *8*. https://doi.org/10.3390/diagnostics8040076.
6. Morse, M.A., Chaudhry, A., Gabitzsch, E.S., Hobeika, A.C., Osada, T., Clay, T.M., Amalfitano, A., Burnett, B.K., Devi, G.R., Hsu, D.S., et al. (2013). Novel adenoviral vector induces T-cell responses despite anti-adenoviral neutralizing antibodies in colorectal cancer patients. Cancer Immunol. Immunother. *62*, 1293–1301. https://doi.org/10.1007/s00262-013-1400-3.
7. Shaw, A.R., and Suzuki, M. (2019). Immunology of adenoviral vectors in cancer therapy. Mol. Ther. Methods Clin. Dev. *15*, 418–429. https://doi.org/10.1016/j.omtm.2019.11.001.
8. O'Connell, P., Pepelyayeva, Y., Blake, M.K., Hyslop, S., Crawford, R.B., Rizzo, M.D., Pereira-Hicks, C., Godbehere, S., Dale, L., Gulick, P., et al. (2018). SLAMF7 is a critical negative regulator of IFN-alpha-Mediated CXCL10 production in chronic HIV infection. J. Immunol. https://doi.org/10.4049/jimmunol.1800847.
9. O'Connell, P., Amalfitano, A., and Aldhamen, Y.A. (2019). SLAM family receptor signaling in viral infections: HIV and beyond. Vaccines (Basel) *7*. https://doi.org/10.3390/vaccines7040184.
10. O'Connell, P., Hyslop, S., Blake, M.K., Godbehere, S., Amalfitano, A., and Aldhamen, Y.A. (2021). SLAMF7 signaling reprograms T cells toward exhaustion in the tumor microenvironment. J. Immunol. *206*, 193–205. https://doi.org/10.4049/jimmunol.2000300.
11. Perez-Quintero, L.A., Roncagalli, R., Guo, H., Latour, S., Davidson, D., and Veillette, A. (2014). EAT-2, a SAP-like adaptor, controls NK cell activation through phospholipase Cgamma, Ca++, and Erk, leading to granule polarization. J. Exp. Med. *211*, 727–742. https://doi.org/10.1084/jem.20132038.
12. Cruz-Munoz, M.E., Dong, Z., Shi, X., Zhang, S., and Veillette, A. (2009). Influence of CRACC, a SLAM family receptor coupled to the adaptor EAT-2, on natural killer cell function. Nat. Immunol. *10*, 297–305. https://doi.org/10.1038/ni.1693.
13. Kim, J.R., Horton, N.C., Mathew, S.O., and Mathew, P.A. (2013). CS1 (SLAMF7) inhibits production of proinflammatory cytokines by activated monocytes. Inflamm. Res. *62*, 765–772. https://doi.org/10.1007/s00011-013-0632-1.
14. Aldhamen, Y.A., Rastall, D.P.W., Chen, W., Seregin, S.S., Pereira-Hicks, C., Godbehere, S., Kaminski, N.E., and Amalfitano, A. (2016). CRACC-targeting Fc-fusion protein induces activation of NK cells and DCs and improves T cell immune responses to antigenic targets. Vaccine *34*, 3109–3118. https://doi.org/10.1016/j.vaccine.2016.04.068.
15. Reilly, R.M., Sandhu, J., Alvarez-Diez, T.M., Gallinger, S., Kirsh, J., and Stern, H. (1995). Problems of delivery of monoclonal antibodies. Pharmaceutical and pharmacokinetic solutions. Clin. Pharmacokinet. *28*, 126–142. https://doi.org/10.2165/00003088-199528020-00004.
16. Samaranayake, H., Wirth, T., Schenkwein, D., Raty, J.K., and Yla-Herttuala, S. (2009). Challenges in monoclonal antibody-based therapies. Ann. Med. *41*, 322–331. https://doi.org/10.1080/07853890802698842.
17. Ngwa, W., Irabor, O.C., Schoenfeld, J.D., Hesser, J., Demaria, S., and Formenti, S.C. (2018). Using immunotherapy to boost the abscopal effect. Nat. Rev. Cancer *18*, 313–322. https://doi.org/10.1038/nrc.2018.6.
18. Watanabe, H., Numata, K., Ito, T., Takagi, K., and Matsukawa, A. (2004). Innate immune response in Th1- and Th2-dominant mouse strains. Shock *22*, 460–466. https://doi.org/10.1097/01.shk.0000142249.08135.e9.
19. Beltra, J.C., Manne, S., Abdel-Hakeem, M.S., Kurachi, M., Giles, J.R., Chen, Z., Casella, V., Ngiow, S.F., Khan, O., Huang, Y.J., et al. (2020). Developmental relationships of four exhausted CD8(+) T cell subsets reveals underlying transcriptional and epigenetic landscape control mechanisms. Immunity *52*, 825–841.e8. https://doi.org/10.1016/j.immuni.2020.04.014.
20. Maier, B., Leader, A.M., Chen, S.T., Tung, N., Chang, C., LeBerichel, J., Chudnovskiy, A., Maskey, S., Walker, L., Finnigan, J.P., et al. (2020). A conserved dendritic-cell regulatory program limits antitumour immunity. Nature *580*, 257–262. https://doi.org/10.1038/s41586-020-2134-y.
21. Cannons, J.L., Tangye, S.G., and Schwartzberg, P.L. (2011). SLAM family receptors and SAP adaptors in immunity. Annu. Rev. Immunol. *29*, 665–705. https://doi.org/10.1146/annurev-immunol-030409-101302.
22. Aldhamen, Y.A., Appledorn, D.M., Seregin, S.S., Liu, C.J., Schuldt, N.J., Godbehere, S., and Amalfitano, A. (2011). Expression of the SLAM family of receptors adapter EAT-2 as a novel strategy for enhancing beneficial immune responses to vaccine antigens. J. Immunol. *186*, 722–732. https://doi.org/10.4049/jimmunol.1002105.
23. Culos, A., Tsai, A.S., Stanley, N., Becker, M., Ghaemi, M.S., McIlwain, D.R., Fallahzadeh, R., Tanada, A., Nassar, H., Espinosa, C., et al. (2020). Integration of mechanistic immunological knowledge into a machine learning pipeline improves predictions. Nat. Mach. Intell. *2*, 619–628. https://doi.org/10.1038/s42256-020-00232-8.
24. Jorgovanovic, D., Song, M., Wang, L., and Zhang, Y. (2020). Roles of IFN-gamma in tumor progression and regression: a review. Biomark. Res. *8*, 49. https://doi.org/10.1186/s40364-020-00228-x.
25. Hegde, S., Leader, A.M., and Merad, M. (2021). MDSC: markers, development, states, and unaddressed complexity. Immunity *54*, 875–884. https://doi.org/10.1016/j.immuni.2021.04.004.
26. Scodeller, P., Simon-Gracia, L., Kopanchuk, S., Tobi, A., Kilk, K., Saalik, P., Kurm, K., Squadrito, M.L., Kotamraju, V.R., Rinken, A., et al. (2017). Precision targeting of tumor macrophages with a CD206 binding peptide. Sci. Rep. *7*, 14655. https://doi.org/10.1038/s41598-017-14709-x.
27. Feng, Q., Chang, W., Mao, Y., He, G., Zheng, P., Tang, W., Wei, Y., Ren, L., Zhu, D., Ji, M., et al. (2019). Tumor-associated macrophages as prognostic and predictive biomarkers for postoperative adjuvant chemotherapy in patients with stage II colon cancer. Clin. Cancer Res. *25*, 3896–3907. https://doi.org/10.1158/1078-0432.CCR-18-2076.

28. Tugues, S., Burkhard, S.H., Ohs, I., Vrohlings, M., Nussbaum, K., Vom Berg, J., Kulig, P., and Becher, B. (2015). New insights into IL-12-mediated tumor suppression. Cell Death Differ. *22*, 237–246. https://doi.org/10.1038/cdd.2014.134.

29. Fuertes, M.B., Woo, S.R., Burnett, B., Fu, Y.X., and Gajewski, T.F. (2013). Type I interferon response and innate immune sensing of cancer. Trends Immunol. *34*, 67–73. https://doi.org/10.1016/j.it.2012.10.004.

30. Musella, M., Manic, G., De Maria, R., Vitale, I., and Sistigu, A. (2017). Type-I-interferons in infection and cancer: unanticipated dynamics with therapeutic implications. Oncoimmunology *6*, e1314424. https://doi.org/10.1080/2162402X.2017.1314424.

31. Way, S.S., Havenar-Daughton, C., Kolumam, G.A., Orgun, N.N., and Murali-Krishna, K. (2007). IL-12 and type-I IFN synergize for IFN-gamma production by CD4 T cells, whereas neither are required for IFN-gamma production by CD8 T cells after Listeria monocytogenes infection. J. Immunol. *178*, 4498–4505. https://doi.org/10.4049/jimmunol.178.7.4498.

32. Melero, I., Mazzolini, G., Narvaiza, I., Qian, C., Chen, L., and Prieto, J. (2001). IL-12 gene therapy for cancer: in synergy with other immunotherapies. Trends Immunol. *22*, 113–115. https://doi.org/10.1016/s1471-4906(00)01824-x.

33. Fitzgerald-Bocarsly, P., Dai, J., and Singh, S. (2008). Plasmacytoid dendritic cells and type I IFN: 50 years of convergent history. Cytokine Growth Factor Rev. *19*, 3–19. https://doi.org/10.1016/j.cytogfr.2007.10.006.

34. Quatrini, L., Mariotti, F.R., Munari, E., Tumino, N., Vacca, P., and Moretta, L. (2020). The immune checkpoint PD-1 in natural killer cells: expression, function and targeting in tumour immunotherapy. Cancers (Basel) *12*. https://doi.org/10.3390/cancers12113285.

35. Chevrier, S., Levine, J.H., Zanotelli, V.R.T., Silina, K., Schulz, D., Bacac, M., Ries, C.H., Ailles, L., Jewett, M.A.S., Moch, H., et al. (2017). An immune atlas of clear cell renal cell carcinoma. Cell *169*, 736–749.e18. https://doi.org/10.1016/j.cell.2017.04.016.

36. Jager, L., Hausl, M.A., Rauschhuber, C., Wolf, N.M., Kay, M.A., and Ehrhardt, A. (2009). A rapid protocol for construction and production of high-capacity adenoviral vectors. Nat. Protoc. *4*, 547–564. https://doi.org/10.1038/nprot.2009.4.

37. Aldhamen, Y.A., Seregin, S.S., Aylsworth, C.F., Godbehere, S., and Amalfitano, A. (2014). Manipulation of EAT-2 expression promotes induction of multiple beneficial regulatory and effector functions of the human innate immune system as a novel immunomodulatory strategy. Int. Immunol. *26*, 291–303. https://doi.org/10.1093/intimm/dxt061.

38. Herr, W., Ranieri, E., Olson, W., Zarour, H., Gesualdo, L., and Storkus, W.J. (2000). Mature dendritic cells pulsed with freeze-thaw cell lysates define an effective in vitro vaccine designed to elicit EBV-specific CD4(+) and CD8(+) T lymphocyte responses. Blood *96*, 1857–1864.

39. Alyaqoub, F.S., Aldhamen, Y.A., Koestler, B.J., Bruger, E.L., Seregin, S.S., Pereira-Hicks, C., Godbehere, S., Waters, C.M., and Amalfitano, A. (2016). In vivo Synthesis of cyclic-di-GMP using a recombinant adenovirus preferentially improves adaptive immune responses against extracellular antigens. J. Immunol. https://doi.org/10.4049/jimmunol.1501272.

40. Chevrier, S., Crowell, H.L., Zanotelli, V.R.T., Engler, S., Robinson, M.D., and Bodenmiller, B. (2018). Compensation of signal spillover in suspension and imaging mass cytometry. Cell Syst. *6*, 612–620.e5. https://doi.org/10.1016/j.cels.2018.02.010.

41. Aldhamen, Y.A., Seregin, S.S., Schuldt, N.J., Rastall, D.P., Liu, C.J., Godbehere, S., and Amalfitano, A. (2012). Vaccines expressing the innate immune modulator EAT-2 elicit potent effector memory T lymphocyte responses despite pre-existing vaccine immunity. J. Immunol. *189*, 1349–1359. https://doi.org/10.4049/jimmunol.1200736.

42. DeTomaso, D., Jones, M.G., Subramaniam, M., Ashuach, T., Ye, C.J., and Yosef, N. (2019). Functional interpretation of single cell similarity maps. Nat. Commun. *10*, 4376. https://doi.org/10.1038/s41467-019-12235-0.

43. Appledorn, D.M., Aldhamen, Y.A., Depas, W., Seregin, S.S., Liu, C.J., Schuldt, N., Quach, D., Quiroga, D., Godbehere, S., Zlatkin, I., et al. (2010). A new adenovirus based vaccine vector expressing an Eimeria tenella derived TLR agonist improves cellular immune responses to an antigenic target. PLoS One *5*, e9579. https://doi.org/10.1371/journal.pone.0009579.

44. Seregin, S.S., Aldhamen, Y.A., Appledorn, D.M., Hartman, Z.C., Schuldt, N.J., Scott, J., Godbehere, S., Jiang, H., Frank, M.M., and Amalfitano, A. (2010). Adenovirus capsid-display of the retro-oriented human complement inhibitor DAF reduces Ad vector-triggered immune responses in vitro and in vivo. Blood *116*, 1669–1677. https://doi.org/10.1182/blood-2010-03-276949.

45. Seregin, S.S., Appledorn, D.M., Patial, S., Bujold, M., Nance, W., Godbehere, S., Parameswaran, N., and Amalfitano, A. (2010). beta-Arrestins modulate Adenovirus-vector-induced innate immune responses: differential regulation by beta-arrestin-1 and beta-arrestin-2. Virus Res. *147*, 123–134. https://doi.org/10.1016/j.virusres.2009.10.023.

46. Appledorn, D.M., Aldhamen, Y.A., Godbehere, S., Seregin, S.S., and Amalfitano, A. (2011). Sublingual administration of an adenovirus serotype 5 (Ad5)-based vaccine confirms toll-like receptor agonist activity in the oral cavity and elicits improved mucosal and systemic cell-mediated responses against HIV antigens despite preexisting Ad5 immunity. Clin. Vaccine Immunol. *18*, 150–160. https://doi.org/10.1128/CVI.00341-10.

OMTO, Volume *24*

Supplemental information

Adenoviral delivery of an immunomodulatory protein to the tumor microenvironment controls tumor growth

Patrick O'Connell, Maja K. Blake, Yuliya Pepelyayeva, Sean Hyslop, Sarah Godbehere, Ariana M. Angarita, Cristiane Pereira-Hicks, Andrea Amalfitano, and Yasser A. Aldhamen

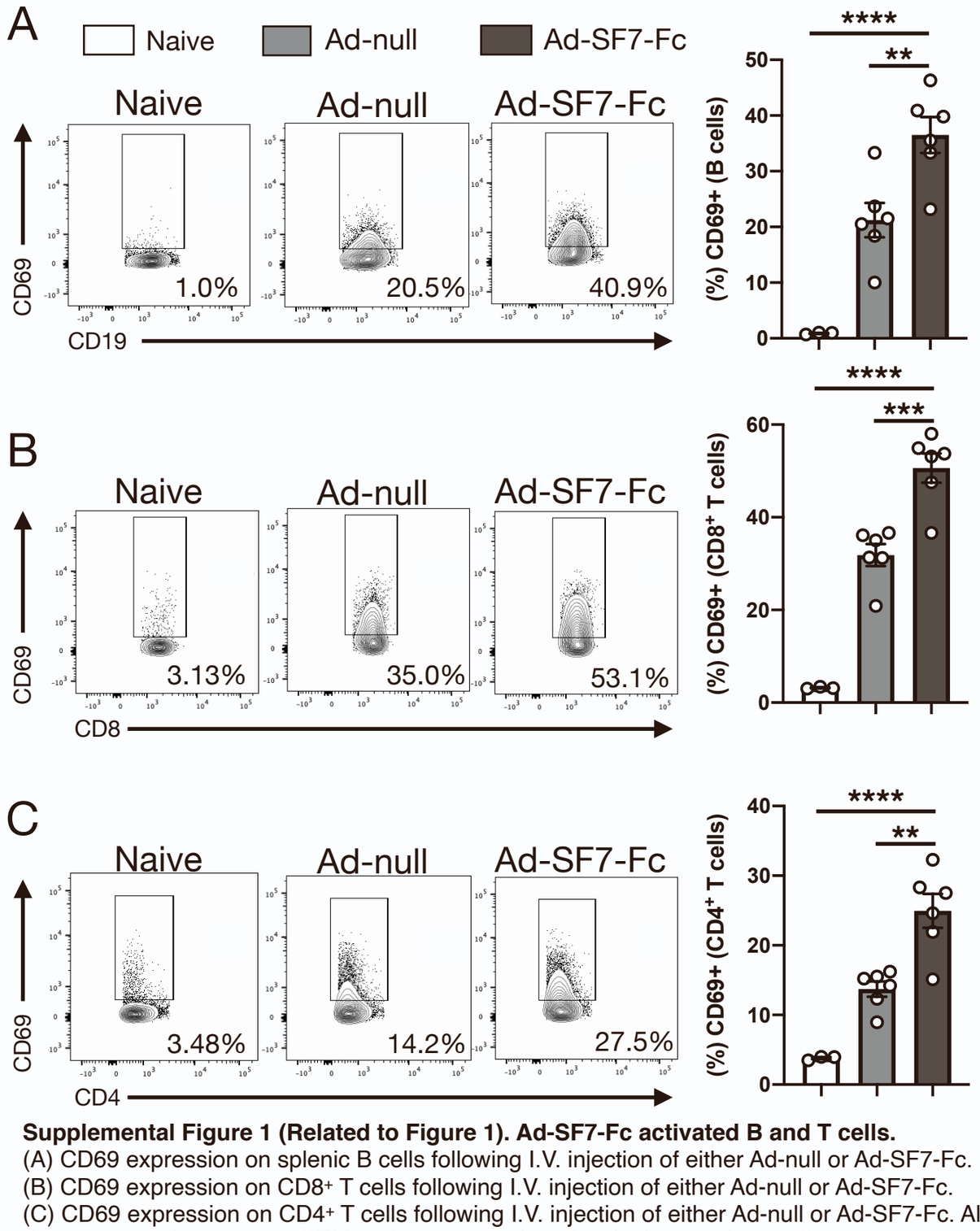

Supplemental Figure 1 (Related to Figure 1). Ad-SF7-Fc activated B and T cells.
(A) CD69 expression on splenic B cells following I.V. injection of either Ad-null or Ad-SF7-Fc. (B) CD69 expression on $CD8^+$ T cells following I.V. injection of either Ad-null or Ad-SF7-Fc. (C) CD69 expression on $CD4^+$ T cells following I.V. injection of either Ad-null or Ad-SF7-Fc. All data presented as mean $\pm$ SEM and representative of a single experiment. Groups compared with one-way ANOVA with Tukey's multiple comparison test. **p<0.01; ***p<0.001; ****p<0.0001.

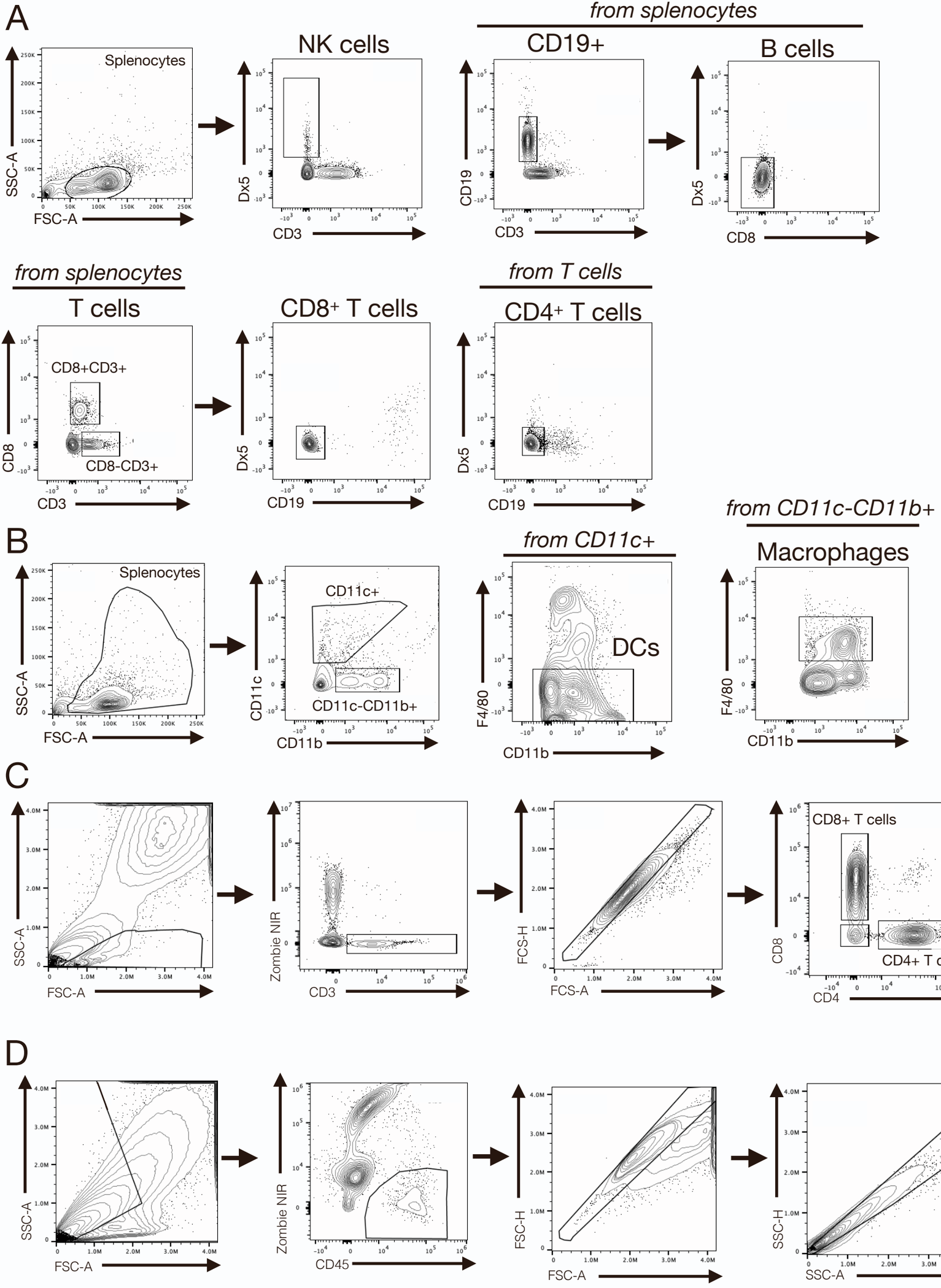

Supplemental Figure 2. Flow cytometry and spectral cytometry gating strategies.
(A) Flow cytometry gating approach used for lymphocytes in Fig. 1 and Supplemental Fig. 1. (B) Flow cytometry gating approach used for myeloid cells in Fig. 1. (C) Spectral cytometry gating approach used for B16 TIL T cell analysis in Fig. 4C-G and Supplemental Fig. 4. (D) Spectral cytometry gating approach used for B16 high dimensional TME profiling in Fig. 4H-J, Fig. 5, Fig. 7, Supplemental Fig. 5, and Supplemental Fig. 6. We utilized a broad-based strategy so as to capture all tumor-infiltrating immune cells, and cleaned up data with an additional singlet gate.

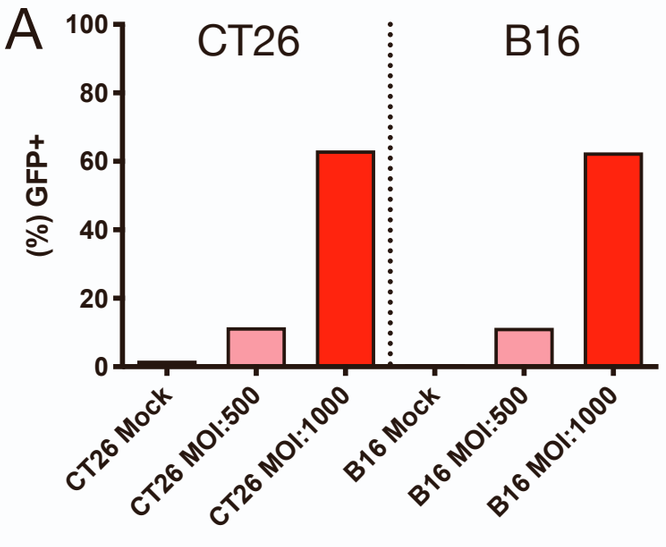

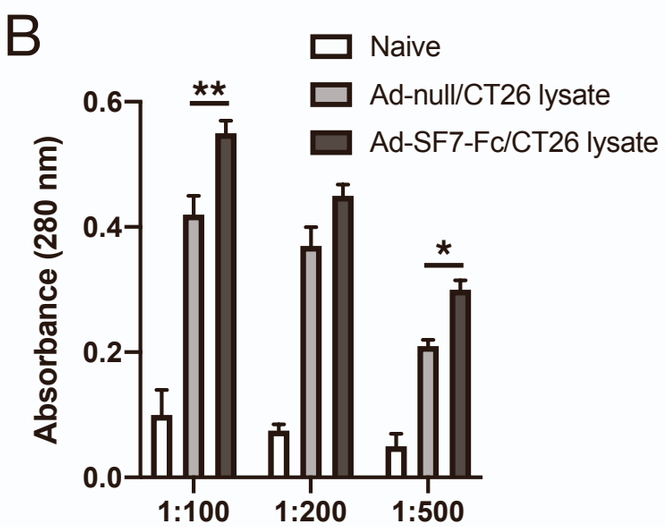

Supplemental Figure 3 (Related to Figure 3). CT26-specific IgG responses following adenovirus vaccination and Ad infection testing of CT26 and B16. (A) CT26 and B16 tumor cells were infected in vitro for 18 hrs with varying MOI's of Ad-GFP to determine optimal dose for tumor cell transduction and treatment. (B) Relative abundance of tumor specific IgG antibodies in plasma of non-vaccinated (naive) (n=2), Ad-null/CT26 lysate (n=6), and Ad-SF7-Fc/CT26 lysate (n=7) vaccinated mice using different dilutions. All data presented as mean ± SEM and representative of a single experiment. Groups compared with one-way ANOVA with Tukey's multiple comparison test. *p<0.05; **p<0.01.

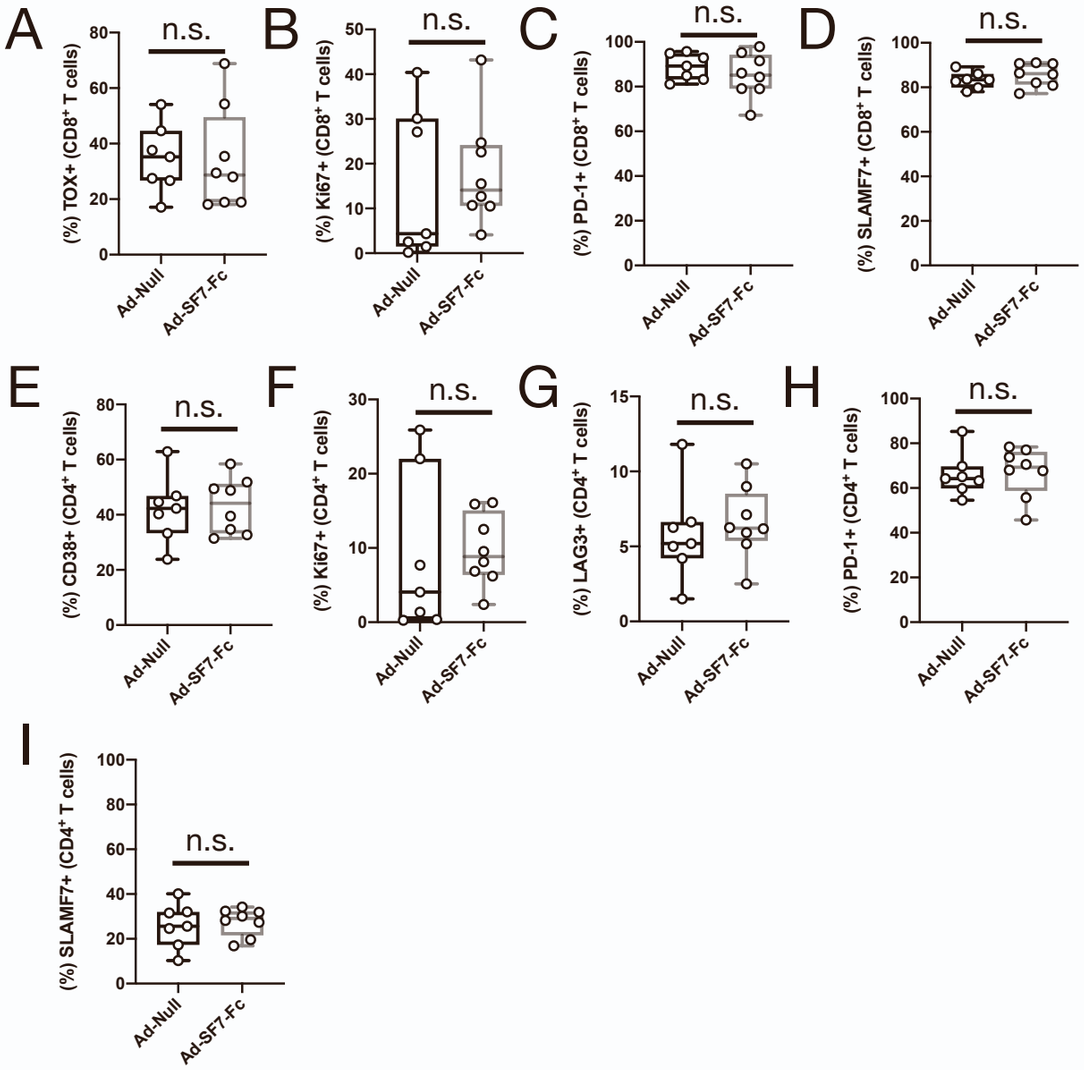

Supplemental Figure 4 (Related to Figure 4). CD4⁺ and CD8⁺ B16 TIL phenotypes from adenovirus treated mice.

(A) Frequency of TOX⁺ CD8⁺ TILs between Ad-null and Ad-SF7-Fc treated B16 tumors. (B) Frequency of Ki67⁺ CD8⁺ TILs between Ad-null and Ad-SF7-Fc treated B16 tumors.

(C) Frequency of PD-1⁺ CD8⁺ TILs between Ad-null and Ad-SF7-Fc treated B16 tumors. (D) Frequency of SLAMF7⁺ CD8⁺ TILs between Ad-null and Ad-SF7-Fc treated B16 tumors. (E) Frequency of CD38⁺ CD4⁺ TILs between Ad-null and Ad-SF7-Fc treated B16 tumors. (F) Frequency of Ki67⁺ CD4⁺ TILs between Ad-null and Ad-SF7-Fc treated B16 tumors. (G) Frequency of LAG3⁺ CD4⁺ TILs between Ad-null and Ad-SF7-Fc treated B16 tumors. (H) Frequency of PD-1⁺ CD4⁺ TILs between Ad-null and Ad-SF7-Fc treated B16 tumors. (I) Frequency of SLAMF7⁺ CD4⁺ TILs between Ad-null and Ad-SF7-Fc treated B16 tumors.

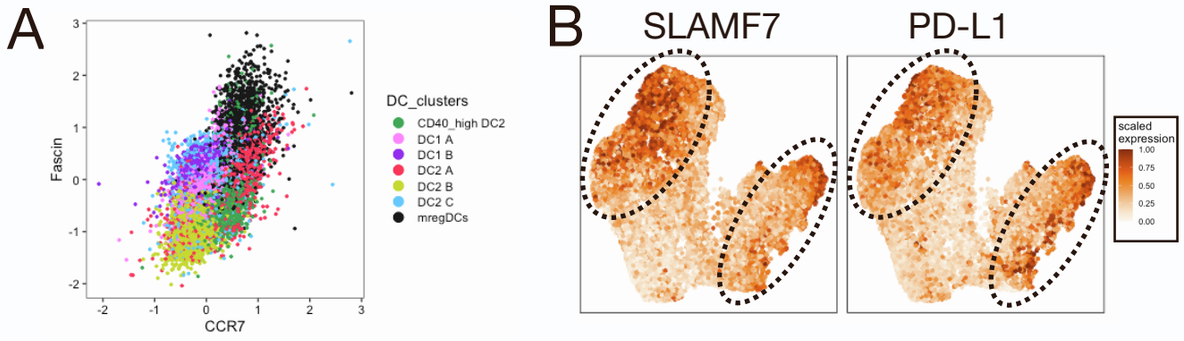

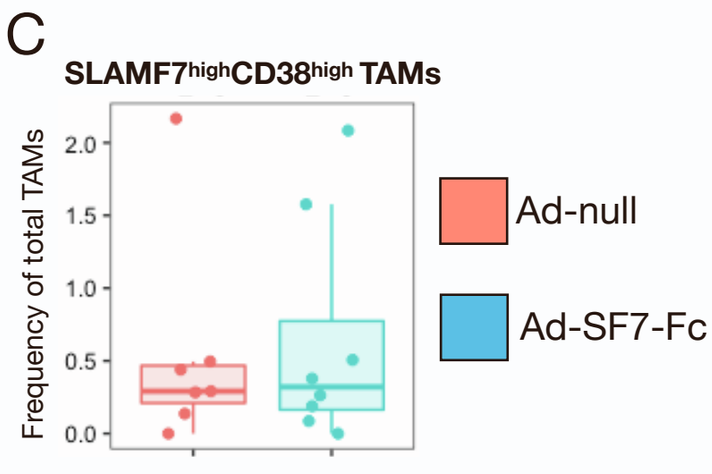

Supplemental Figure 5 (Related to Figure 5). mregDC identification and SLAMF7/PD-L1 co-expression on TAMs.
(A) Dot plot of Fascin and CCR7 co-expression on DC subsets from adenovirus treated tumors. Points are colored by DC subset. mregDCs are defined by high co-expression of both of these markers.18 (B) Expression of SLAMF7 and PD-L1 overlaid onto UMAP plot of TAM subsets as depicted in Figure 5G. (C) Frequency of SLAMF7^{high}CD38^{high} TAMs between Ad-null and Ad-SF7-Fc treated B16 tumors.

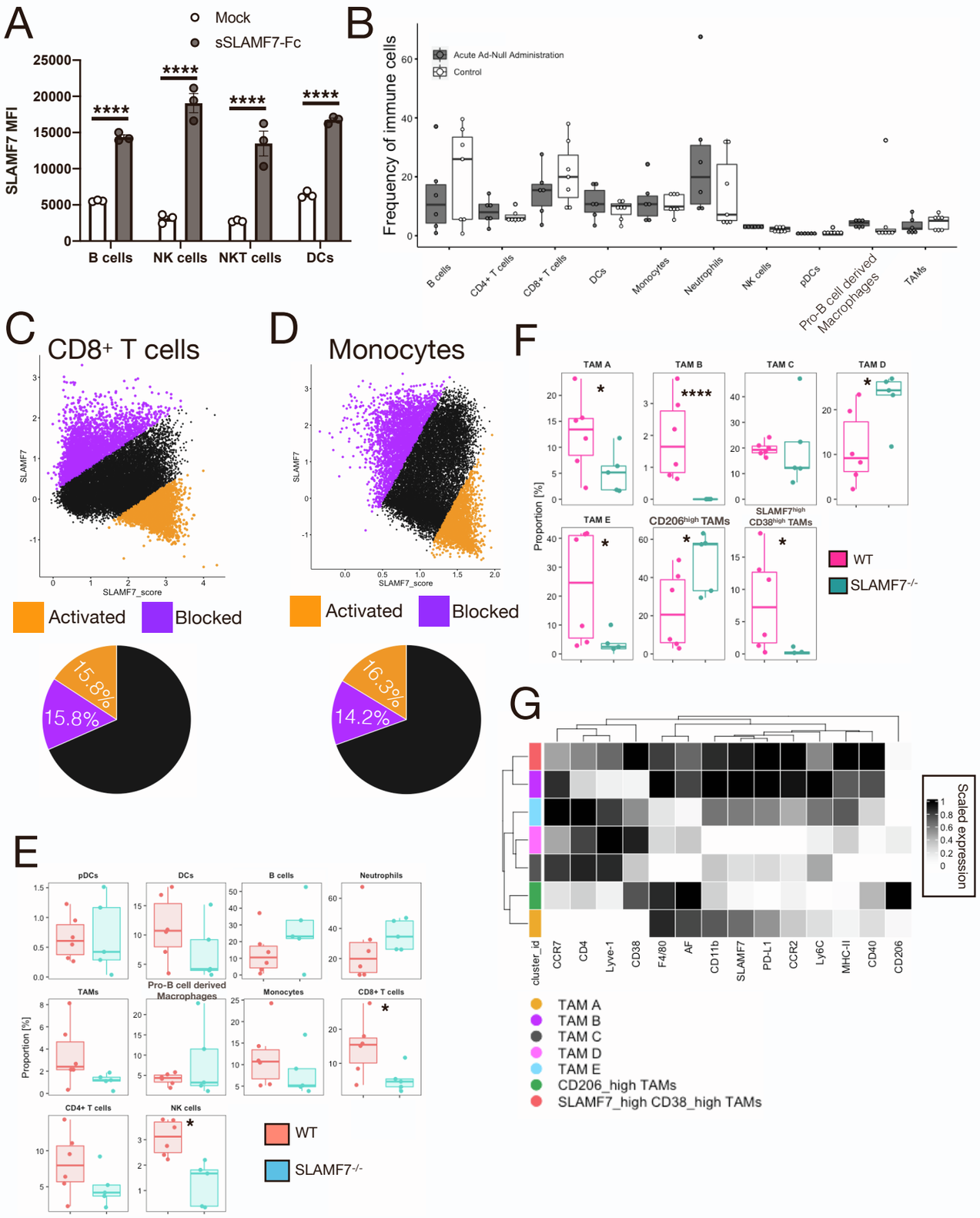

Supplemental Figure 6 (Related to Figure 7). Supporting data for SF7-Fc predictions and TME changes in B16 tumors of SLAMF7$^{-/-}$ mice.
(A) Expression of SLAMF7 on splenic immune cell subsets from WT mice, in vitro stimulated with 10 μg/mL soluble SLAMF7-Fc protein (sSLAMF7-Fc) for two days. (B) Frequency of TME immune cell subsets between mice who received a single injection of Ad-null at day 7 post B16 tumor inoculation (Control) and mice who also received a second injection 24 hrs before sacrifice (Acute Ad Null Administration). Activating versus blocking predictions of SF7-Fc in CD8^{+} T cells (C) and Monocytes (D) depicted as in Fig. 7B-E. (E) Frequency of tumor-infiltrating immune cell subsets from B16 tumors of WT (Ad-null) and SLAMF7$^{-/-}$ (Ad-null) mice assessed by spectral cytometry similarly to Fig. 4J. (F) Frequency of TAM subsets from B16 tumors between WT (Ad-null) and SLAMF7$^{-/-}$ (Ad-null) mice. (G) Marker expression on TAM subsets from (F). Data in (A, F-G) representative of a single experiment. Data in (B) aggregated from multiple experiments. Data in (C and D) representative of two independent experiments showing similar results. Data in (A) presented as mean $\pm$ SEM and groups compared with two-way ANOVA with Sidak's multiple comparison test. Groups in (E and F) compared with a GLMM. *p<0.05; ****p<0.0001. AF; autofluorescence.

Supplemental table 2. iEN model coefficients. Only non-0 coefficients are included.

Feature	Beta	Interpretation
CD8+ T cells	0.636777322	Inc. in responders
PD-L1_TAMs	0.576284123	Inc. in responders
B220_B cells	0.574742634	Inc. in responders
IL_12p40_lysate	0.429617979	Inc. in responders
SLAMF7_TAMs	0.3491533	Inc. in responders
IgD_B cells	0.278947827	Inc. in responders
CD11c_TAMs	0.272528427	Inc. in responders
Tex_prog1	0.207656434	Inc. in responders
Ly6C_pDCs	0.195718603	Inc. in responders
Pro-B cell derived Macrophages	0.193926537	Inc. in responders
IL_10_lysate	0.181000311	Inc. in responders
IFNg_lysate	0.177540472	Inc. in responders
TAMs_activated	0.160726842	Inc. in responders
MIP_1a_lysate	0.154900386	Inc. in responders
MCP_1_lysate	0.136453361	Inc. in responders
CD45_TAMs	0.134739305	Inc. in responders
Ly6C_CD8+ T cells	0.134206359	Inc. in responders
TOX+_CD8	0.115547706	Inc. in responders
IL_6_lysate	0.114914635	Inc. in responders
SLAMF7_DCs	0.098996632	Inc. in responders
Tex_int	0.079320436	Inc. in responders
pDCs_activated	0.076432825	Inc. in responders
PD-L1_Pro-B cell derived Macrophages	0.059414611	Inc. in responders
MHC-II_TAMs	0.058278209	Inc. in responders
CCR2_TAMs	0.053394087	Inc. in responders
CD8_T_cells_activated	0.043799318	Inc. in responders
GM_CSF_lysate	0.0425075	Inc. in responders
Eotaxin_lysate	0.041849572	Inc. in responders
B220_Pro-B cell derived Macrophages	0.033258237	Inc. in responders
CD38_B cells	0.02633125	Inc. in responders
CD11b_TAMs	0.021632477	Inc. in responders

AF_B cells	0.021309016	Inc. in responders
Ly6G_Neutrophils	0.021267713	Inc. in responders
MIP_1b_lysate	0.021107824	Inc. in responders
PD-1_CD8+ T cells	0.015923065	Inc. in responders
CD90_CD8+ T cells	0.013698046	Inc. in responders
CD11c_NK cells	0.011434616	Inc. in responders
TNF_a_plasma_day1	0.010473118	Inc. in responders
CD90_CD4+ T cells	0.010203013	Inc. in responders
IL_3_lysate	0.009106385	Inc. in responders
G_CSF_lysate	0.008431265	Inc. in responders
TOX_high_PD1_high_CD8	0.007180879	Inc. in responders
CCR2_DCs	0.006887445	Inc. in responders
IL_4_lysate	0.004009159	Inc. in responders
MHC-II_DCs	0.003805041	Inc. in responders
CCR2_Monocytes	0.003246796	Inc. in responders
CD90_NK cells	0.000369813	Inc. in responders
CCL5_plasma_day0	-0.017050343	Dec. in responders
TAMs	-0.019593439	Dec. in responders
CD206_TAMs	-0.02316422	Dec. in responders
CD38_pDCs	-0.025184203	Dec. in responders
IL_4_plasma_day0	-0.034607044	Dec. in responders
Tex_prog2	-0.043115321	Dec. in responders
TNF_a_plasma_day0	-0.056736883	Dec. in responders
IL_1b_plasma_day0	-0.136661524	Dec. in responders
IL_12p70_lysate	-0.1835637	Dec. in responders
Neutrophils	-0.229220797	Dec. in responders
Lyve-1_Pro-B cell derived Macrophages	-0.236662769	Dec. in responders
IL_12p40_plasma_day0	-0.325532592	Dec. in responders
B220_pDCs	-0.335022487	Dec. in responders
IL_1a_lysate	-0.38754388	Dec. in responders

Supplemental table 3. List of all antibodies used.

Antibody	Conjugate	Source
CD3 (clone 145-2C11)	APC	BD Biosciences
CD38 (clone 90/CD38)	BV510	BD Biosciences
CD8a (clone 53-6.7)	Alexa 700	Thermofisher
CD11c (clone HL3)	PE-Cy7	BD Biosciences
CD11b (clone M1/70)	APC-Cy7	BD Biosciences
F4/80 (Clone BMB)	PE	Thermofisher
CD86 (Clone GL1)	V450	BD Biosciences
CD3e (clone SK7)	APC-Cy7	BD Biosciences
CD19 (clone 1D3)	PerCp-Cy5.5	BD Biosciences
Dx5 (a.k.a. CD49b)	PE-Cy7	Thermofisher
CD69 (clone H1.2F3)	FITC	BD Biosciences
IFNg (clone XMG1.2)	Alexa 488	BD Biosciences
CD45 (clone 30-F11)	Alexa 532	Thermofisher
CD11b (clone M1/70)	BV570	BioLegend
CD4 (clone RM4-5)	eFluor450	Thermofisher
NK1.1 (clone PK136)	PE-Cy7	Thermofisher
SLAMF7 (clone 4G2)	APC	BioLegend
Ly6C (clone HK1.4)	BV421	BioLegend
Zombie NIR (viability)	N/A	BioLegend
Ly6G (clone 1A8)	BV711	BioLegend
MHC-II (clone M4/114.15.2)	BV785	BioLegend
CD3 (clone 17A2)	BUV737	BD Biosciences
CD11c (clone HL3)	PE-CF594	BD Biosciences
B220 (clone RA3-6B2)	BV480	BD Biosciences
IgD (clone 11-26c)	SuperBright 436	Thermofisher
CD206 (clone C06802)	Alexa 647	BioLegend
CCR2 (clone 747967)	BV750	BD Biosciences
Lyve1 (clone ALY7)	eFluor615	Thermofisher
CD90.2 (clone 53-2.1)	BUV396	BD Biosciences
PD-1 (clone RMP1-30)	PerCp-eFluor710	Thermofisher
LAG3 (clone C9B7W)	BV785	BioLegend

Ki67 (clone B56)	BV421	BD Biosciences
2B4 (clone m2B4 (B6)458.1)	FITC	BioLegend
TOX (clone TXRX10)	eFluor660	Thermofisher
SLAMF6 (clone 13B3)	BUV395	BD Biosciences
CD69 (clone H1.2F3)	PE-Cy7	BD Biosciences
CD40 (clone 3/23)	APC-Fire750	BioLegend
Fascin (clone 55K-2)	Alexa 488	Santa Cruz Biotech
CCR7 (clone 4B12)	BV605	BD Biosciences
PD-L1 (clone 10F.9G2)	BV650	BD Biosciences
EAT-2 (clone LS-C87204)	Alexa647	LSBio

Supplemental table 4. IHC antibodies and staining specifications.

Primary Ab	Vendor	Pretreatment	Primary	Staining system (BioCare Medical)
Rabbit anti – CD3 Polyclonal	Abcam #GR3194253-3 Cambridge, MA	Heat Retrieval – Citrate Buffer pH 6.0 – Pascal Pressure Cooker – 125°C for 15 sec, 80°C for 1 min, room temperature with lid off for 30 min	1:450 in NAD – 1 Hour	Rodent Block M – 20 minutes ProMark Rabbit on Rodent HRP PolymerTM - 35 minutes AEC Chromogen – 5 minutes CATHE Hematoxylin 1:10 – 1 minute
Rat anti – CD8 Monoclonal	Dianova *#DIA-808* Hamburg, Germany	Heat Retrieval – Citrate Buffer pH 6.0 – Steamer for 30 min, room temperature with lid off for 10 min	1:100 in NAD - 1 Hour	Rodent Block M – 10 minutes ProMark Rat on Mouse HRP ProbeTM - 10 minutes ProMark Rat on Mouse HRP PolymerTM - 10 minutes AEC Chromogen – 5 minutes CATHE Hematoxylin 1:10 – 1 minute
Rabbit anti – Integrin Alpha 2 (DX5) Monoclonal	Abcam #GR196223-25 Cambridge, MA	No Pretreatment	1:100 in NAD – 1 Hour	Rodent Block M – 20 minutes ProMark Rabbit on Rodent HRP PolymerTM - 20 minute AEC Chromogen – 5 minutes CATHE Hematoxylin 1:10 – 1 minute